

# Active Site Spectral Studies on Manganese Superoxide Dismutase

James W. Whittaker\* and Mei M. Whittaker

Contribution from the Department of Chemistry, Carnegie Mellon University, 4400 Fifth Avenue, Pittsburgh, Pennsylvania 15213. Received December 17, 1990

**Abstract:** Manganese superoxide dismutase from *Escherichia coli* has been prepared in homogeneous Mn<sup>3+</sup> and Mn<sup>2+</sup> redox forms for characterization by a combination of optical absorption, circular dichroism (CD), magnetic circular dichroism (MCD), and EPR spectroscopies. MCD spectra of the unliganded Mn<sup>3+</sup> protein displays a strikingly simple pattern, a pair of bands of equal magnitude but oppositely signed intensity. Saturation magnetization curves for the native Mn site show a dramatic nesting that reflects large splittings in the paramagnetic ground state, suggesting positive zero-field splitting ( $D > 0$ ). The ground-state behavior and the excited-state spectra can be interpreted in terms of a distorted trigonal-bipyramidal environment for the metal ion. Binding exogenous ligands (F<sup>-</sup>, N<sub>3</sub><sup>-</sup>) perturbs the Mn<sup>3+</sup> site, leading to a distinctly different pattern of MCD intensity, a pseudo-A-term feature at high energy that exhibits a strong magnetic field saturation at low temperature. Saturation magnetization curves for the anion complexes are less broadly nested than for the native enzyme and appear to arise from a rhombically split non-Kramers doublet lowest in the quintet ground state ( $D < 0$ ). A change in the nature of the orbital ground state evidently occurs as a consequence of the metal complex distorting when small molecules coordinate. A Berry pseudorotation model is presented for the distorting Mn<sup>3+</sup> site to account for the spectroscopic changes associated with anion binding. On reduction, absorption and CD signals are lost for the Mn center, but weak temperature-dependent MCD features are observed for the d<sup>5</sup> metal ion, providing a probe of the enzyme in this redox form. The reduced active site also responds to anion interactions, reflected in the EPR spectra for the Mn<sup>2+</sup> center, suggesting that small molecules coordinate to both oxidized and reduced metal centers in MnSD.

Manganese is known to be essential for life, appearing in diverse biochemical roles ranging from noncatalytic binding and activation in lectins<sup>1</sup> to water oxidation catalysis in the photosynthetic reaction centers of green plants.<sup>2</sup> Although it is rarer in metalloproteins than either iron or copper, which together constitute more than 90% of known biological transition-metal centers, the absolute requirement for manganese in biochemical processes<sup>3</sup> implies that it forms important functional complexes. However, in contrast to the large number of extensively studied iron and copper metalloproteins, manganese active sites are just beginning to be studied in molecular detail.<sup>1,4</sup> One particularly well studied manganese metalloenzyme is the manganese-containing superoxide dismutase (MnSD) isolated from prokaryotes<sup>5,6</sup> and mitochondria.<sup>7</sup> As a result of broad interest in superoxide dismutases,<sup>8</sup> a wealth of basic biochemical and spectroscopic characterization has been reported for MnSD and a crystal structure is emerging, defining the Mn active site at close to atomic resolution.<sup>9,10</sup> No other catalytic manganese site is this well known. The simplicity of a mononuclear metal center and the availability of high-resolution crystallographic information on its coordination geometry make this an attractive starting point for developing detailed insights into the structures and interactions of Mn sites in proteins from a combination of absorption, circular dichroism (CD), magnetic circular dichroism (MCD), and EPR spectroscopies. We will report here our first results for this program, the preparation and spectroscopic characterization of pure Mn<sup>2+/3+</sup> redox forms of SD and their ligand interactions. The results of these investigations can be expected to provide a basis for characterization of Mn sites in the growing class of important and interesting manganese metalloproteins.

## Materials and Methods

**Biochemical Preparations.** *Escherichia coli* strain AB 2463/pDT1-5, which contains an antibiotic resistance plasmid carrying the MnSD structural gene,<sup>11</sup> was a generous gift from Dr. Danièle Touati, Institut Jacques Monod, Centre National de la Recherche Scientifique, Université Paris VII. *E. coli* pDT1-5 was grown at 37 °C in 20 L of well-aerated 2X LB medium supplemented with 40 mg of MnSO<sub>4</sub>·H<sub>2</sub>O and 50 µg of ampicillin/mL. After the optical density of the culture medium at 600 nm reached 0.3, an additional 100 µg/mL of ampicillin was added hourly. Cells were harvested in late log phase and frozen rapidly in liquid nitrogen.

Superoxide dismutase activity was assayed by using the xanthine oxidase/cytochrome *c* inhibition assay.<sup>12</sup> MnSD was purified by a modification of a previously reported procedure,<sup>3</sup> eliminating heat treatment and streptomycin precipitation steps. The protein pellet obtained from ammonium sulfate fractionation was resuspended and dialyzed overnight against 5 mM potassium phosphate, pH 7.8, and then loaded onto an anion exchange cellulose (Whatman DE-52) equilibrated with the same buffer. The protein fractions flowing directly through the column were concentrated and dialyzed against 2 mM potassium acetate, pH 5.5. The pH of the dialysate was carefully adjusted to 5.5 with 2 mM acetic acid, and the sample was loaded onto a Whatman CM-52 cation exchange chromatography column equilibrated in the same buffer. Protein was eluted with a linear gradient of 2–200 mM potassium acetate buffer, pH 5.5, and the third major protein and activity peak was collected, representing homogeneous MnSD. Protein concentration was routinely determined for the pure MnSD from 280-nm absorption measurements, by using the previously reported molar extinction coefficient,<sup>13</sup>  $E^{1\%}(280 \text{ nm}) = 18.9 \text{ cm}^{-1} (\epsilon_{280} = 8.66 \times 10^4 \text{ M}^{-1} \text{ cm}^{-1})$ . The metal content was determined by atomic absorption spectrometry. Nondenaturing polyacrylamide gel electrophoresis was used to identify mixed-metal Fe/Mn hybrid protein contaminants following the procedure of Fridovitch.<sup>14,15</sup>

- (1) Becker, J. W.; Reeke, G. N., Jr.; Wang, J. L.; Cunningham, B. A.; Edelman, G. M. *J. Biol. Chem.* **1975**, *250*, 1513–1524.
- (2) Babcock, G. T. In *New Comprehensive Biochemistry-Photosynthesis*; Amesz, J., Ed.; Elsevier: New York, 1987; pp 125–158.
- (3) Keen, C. L.; Lönnerdal, B.; Hurley, L. S. In *Biochemistry of the Essential Ultratrace Elements*; Frieden, E., Ed.; Plenum: New York, 1984; pp 89–132.
- (4) Antanaitis, B. C.; Brown, R. D., III; Chasteen, N. D.; Freedman, J. H.; Koenig, S. H.; Lilienthal, H. R.; Peisach, J.; Brewer, C. F. *Biochemistry* **1987**, *26*, 7932–7937.
- (5) Keele, B. B., Jr.; McCord, J. M.; Fridovich, I. *J. Biol. Chem.* **1970**, *245*, 6176–6181.
- (6) Lumsden, J.; Cammack, R.; Hall, D. O. *Biochim. Biophys. Acta* **1976**, *438*, 380–392.
- (7) McCord, J. M.; Boyle, J. A.; Day, E. D., Jr.; Rizzolo, L. J.; Salin, M. L. In *Superoxide and Superoxide Dismutases*; Michelson, A. M., McCord, J. M., Fridovich, I., Eds.; Academic: New York, 1977; pp 129–138.
- (8) Steinman, H. M. In *Superoxide Dismutase*; Oberly, L. W., Ed.; CRC Press: Boca Raton, 1982; Vol. I, pp 11–68.
- (9) Stallings, W. C.; Patridge, K. A.; Strong, R. K.; Ludwig, M. L. *J. Biol. Chem.* **1984**, *259*, 10695–10699.
- (10) Stallings, W. C.; Patridge, K. A.; Ludwig, M. L. In *Superoxide and Superoxide Dismutase in Chemistry, Biology and Medicine*; Rotilio, G., Ed.; Elsevier: New York, 1986; pp 195–201.
- (11) Touati, D. *J. Bacteriol.* **1983**, *155*, 1078–1087.
- (12) McCord, J. M.; Fridovich, I. *J. Biol. Chem.* **1969**, *244*, 6049–6055.
- (13) Beyer, W. F.; Reynolds, J. A.; Fridovich, I. *Biochemistry* **1989**, *28*, 4403–4409.

\* To whom correspondence should be addressed.

Stable  $\text{Mn}^{3+}\text{SD}$  was prepared by the addition of 1.5 equiv of potassium molybdcyanide to the enzyme solution in 50 mM potassium phosphate buffer, pH 7.0, and incubation at room temperature until the oxidation was complete on the basis of monitoring the progress of the reaction at 475 nm. When no further increase in 475-nm absorption was observed (after approximately 20 min), the solution of enzyme and redox agents was loaded onto a desalting column.

**Reagents and Syntheses.** All reagents for preparation of the culture media and buffers were obtained from commercial sources and used without purification. Chromatography media (DEAE Cellulose DE-52; CM-Cellulose CM-52) were obtained from Whatman Biosystems, Ltd. Ampicillin was purchased from Sigma Chemical Co. Potassium octacyanomolybdate(IV) was synthesized according to the published procedure,<sup>16</sup> and potassium molybdcyanide was prepared from the latter compound by permanganate oxidation.<sup>17</sup> Solutions of potassium molybdcyanide oxidant were standardized by titration with ascorbic acid solution and analyzed for Mo by atomic absorption spectrometry. Manganese pentachloride  $[\text{Et}_4\text{N}]_2[\text{MnCl}_5]$  was synthesized according to published procedures,<sup>18,19</sup> dried under vacuum, and stored in the dark until used.

**Spectroscopic and Analytical Instrumentation.** Optical absorption spectra were collected on a Hitachi U-2000 UV-visible absorption spectrometer interfaced with a microcomputer for data acquisition. EPR spectra were recorded on a Bruker ER300 EPR spectrometer with an X-band microwave bridge and temperature control provided by an Oxford Instruments ESR Model 900 helium flow cryostat (4–100 K) with an Fe(Au)-chromel thermocouple sensor or a nitrogen flow insert (120–300 K) with a chromel-alumel thermocouple sensor for temperature measurement. Metal ion analyses were performed on a Varian Model SpectraAA 20B atomic absorption spectrometer equipped with a GTA-96 graphite furnace for high-sensitivity analytical determinations.

CD and MCD spectra were recorded on an AVIV Associates Model 41DS UV-visible-near-IR-IR spectrometer, which is the result of a custom modification of a Cary 14 absorption spectrometer for polarization spectroscopy. The optics bench of the Cary 14 monochromator is retained in the AVIV 41DS, and chopped light from the exit slit is passed successively through a calcite Glan-Thompson polarizer and a Hinds International quartz piezoelectric modulator driven at 50 kHz. A unique relay optics system developed by AVIV drives six quartz lenses on lead screws in an optical zoom design that corrects for chromatic aberration of the lens elements, maintaining a sub-1-mm focus at the sample and detector over the full spectral range of the instrument (190–2000 nm). The light sources for the spectrometer include a water-cooled 450-W Xe arc lamp for the UV-visible region and a 100-W quartz halogen lamp for visible-IR studies. Light detection is provided by a Hamamatsu R-376 red-sensitive phototube (UV-visible), S-1 photomultiplier (near-IR), and a Judson IR liquid nitrogen cooled InSb photovoltaic photodiode with a 1 mm X 1 mm active area (IR). The spectrometer is fully interfaced with a microcomputer for monochromator control, spectral acquisition, and data analysis, supported by AVIV software. Spectral calibration is provided by 1 mg/mL of camphorsulfonic acid. For MCD applications, an Oxford Instruments SM4-6T Spectromag magnetocryostat provides a high magnetic field (to 6 T) and variable temperature (1.5–300 K) perturbation of the sample, in conjunction with an Oxford Instruments ITC temperature controller. MCD samples are prepared in a cell formed by a pair of quartz disks separated by a 1-mm rubber spacer with a circular bore holding 60  $\mu\text{L}$  of sample. Protein samples for low-temperature MCD are routinely prepared in 50% (v/v) glycerol as glassing solvent. Precautions are taken to test for glycerol perturbation of the sample in room temperature spectra, and the glassy frozen sample is examined for depolarization artifacts by comparing the CD spectrum of a 0.12 M nickel tartarate standard placed before and after the sample in the optical path.<sup>20</sup> Depolarizing samples were thawed and refrozen to give glasses with negligible depolarization. In saturation magnetization studies, data were routinely collected by ramping the magnetization field at a low sweep rate with the field controller of the SM4-6T magnetocryostat, the independence of the result on sweep rate being determined in preliminary experiments. Samples of  $[\text{Et}_4\text{N}]_2[\text{MnCl}_5]$  were prepared for MCD spectroscopy by mulling the powdered compound in mineral oil and pressing it into a thin film between quartz disks.

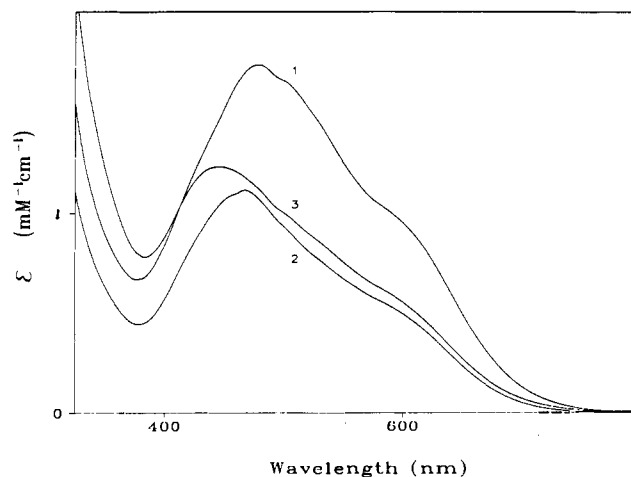


**Figure 1.** Optical absorption spectra of  $\text{Mn}^{3+}$  superoxide dismutase and ligand complexes.  $\text{Mn}^{3+}\text{SD}$  (1 mM active sites), in 50 mM potassium phosphate buffer (pH 7.0): 1, native; 2, in the presence of 400 mM KF; 3, in the presence of 80 mM  $\text{KN}_3$ .

## Results

$\text{MnSD}$  purified by a modification of the published procedures is found to contain stoichiometric Mn ( $0.97 \pm 0.02$  Mn/active site) on the basis of the results of metal ion analysis and protein quantitation using the protein extinction coefficient.<sup>13</sup> These preparations of  $\text{MnSD}$  are homogeneous both in protein and in metal content, with less than 0.02 Fe/active site detected in our samples. The absence of contaminating  $\text{FeSD}$  in this preparation is noteworthy, since during purification of the presence of Mn/Fe hybrid protein can be detected electrophoretically, and the isolation of mixed-metal protein would clearly lead to complications in spectroscopic characterization of the manganese center. The specific activity of the isolated enzyme is found to be 7300 U/mg protein on the basis of the reported UV extinction coefficient.

Initial characterization of freshly isolated, pure  $\text{MnSD}$  by EPR spectroscopy demonstrated an unexpected redox heterogeneity of the active site metal ion. Previous studies have indicated that the enzyme as isolated is in the  $\text{Mn}^{3+}$  oxidation state, the manganic ion contribution the purple color of the protein solutions.<sup>5,21,22</sup> However, these purple samples consistently exhibit an EPR signal at low temperature, which is known to arise from the  $\text{Mn}^{2+}$  form. Addition of dithionite doubles the intensity of the EPR signal, indicating that approximately half of the sites in our samples of  $\text{MnSD}$  are in the  $\text{Mn}^{2+}$  oxidation state, the ratio varying somewhat between preparations, although an earlier report has indicated that freshly isolated  $\text{MnSD}$  is sometimes obtained in an unstable but still homogeneous  $\text{Mn}^{3+}$  form lacking the characteristic EPR signal of  $\text{Mn}^{2+}$  species.<sup>22</sup> There are clear indications that redox heterogeneity is associated with the Mn in superoxide dismutase, perhaps not surprising for a site that undergoes redox cycling in its catalytic mechanism. Similar examples of oxidation state heterogeneity have been observed in other metalloenzymes<sup>23,24</sup> and appear to be particularly likely when redox active metal cofactors are involved.

**Manganic ( $\text{Mn}^{3+}$ ) Superoxide Dismutase. A. Preparation and Spectroscopic Characterization.** The preparation of homogeneous  $\text{Mn}^{3+}$ -containing SD is an essential requirement for detailed spectroscopic studies on the active site, yet no procedure has been reported for the efficient conversion to a homogeneous manganic form. The procedure we have developed involving molybdcyanide oxidation cleanly and efficiently generates homogeneous and stable

(14) Hassan, H. M.; Fridovich, I. *J. Bacteriol.* **1977**, *129*, 1574–1583.

(15) Schiavone, J. R.; Hassan, H. M. *J. Biol. Chem.* **1988**, *263*, 4269–4273.

(16) Furman, N. H.; Miller, C. O. *Inorg. Synth.* **1950**, *3*, 160–163.

(17) Kolthoff, I. M.; Tomsicek, W. J. *J. Phys. Chem.* **1936**, *40*, 247–255.

(18) Goodwin, H. A.; Sylva, R. N. *Aust. J. Chem.* **1965**, *18*, 1743–1749.

(19) Davis, T. S.; Fackler, J. P.; Weeks, M. J. *Inorg. Chem.* **1968**, *7*, 1994–2002.

(20) Browett, W. R.; Fucaloro, A. F.; Morgan, T. V.; Stephens, P. J. *J. Am. Chem. Soc.* **1983**, *105*, 1868–1872.

(21) Keele, B. B., Jr.; Giovagnoli, C.; Rotillio, G. *Physiol. Chem. Physics* **1975**, *7*, 1–6.

(22) Fee, J. A.; Shapiro, E. R.; Moss, T. H. *J. Biol. Chem.* **1976**, *251*, 6157–6159.

(23) Whittaker, M. M.; Whittaker, J. W. *J. Biol. Chem.* **1988**, *263*, 6074–6080.

(24) Khangulov, S. V.; Barynin, V. V.; Antonyuk-Barynina, S. V. *Biochim. Biophys. Acta* **1990**, *1020*, 25–33.

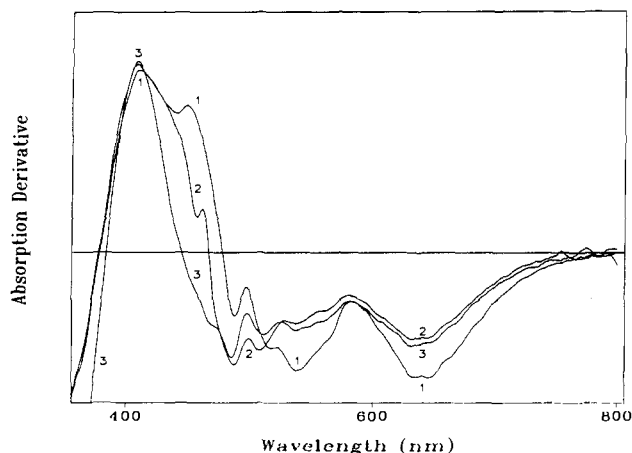


**Figure 2.** First-derivative optical absorption spectra of  $\text{Mn}^{3+}$  superoxide dimutase. Conditions same as for Figure 1: 1, native; 2, in presence of 400 mM KF; 3, in presence of 80 mM  $\text{KN}_3$ .

$\text{Mn}^{3+}$ SD without loss of metal or significant damage to the protein. In particular, oxidation by molybdicyanide does not affect enzyme activity. Curiously, weaker oxidants that we have tried are unable to convert the enzyme to a pure  $\text{Mn}^{3+}$  form, even in the presence of organic mediator dyes, although the redox potential of the Mn site is known<sup>25</sup> to be relatively low ( $E^\circ = 0.31$  V vs NHE) and, thermodynamically, oxidation by ferricyanide should be possible. There seem to be special requirements for this site, limiting the range of effective oxidants, and we find that a slightly more powerful oxidant, hexachloroiridate  $\text{Na}_2\text{IrCl}_6$ , appears to result in irreversible damage to the protein.

Having preparations of pure  $\text{Mn}^{3+}$ SD has made possible an improved determination of the optical absorption features of this form of the enzyme. An absorption spectrum of homogeneous manganic SD is shown in Figure 1. The basic appearance of this spectrum is similar to that previously reported,<sup>5,21,22,26</sup> and the extinction coefficient ( $\epsilon_{478}^{\text{Mn}} = 850 \text{ M}^{-1} \text{ cm}^{-1}$ ) calculated for this sample on the basis of the protein extinction coefficient at 280 nm and corrected molecular weight (45 800 g/mol)<sup>13</sup> is similar to the highest previously reported,<sup>23</sup> reflecting the homogeneity of our  $\text{Mn}^{3+}$ SD preparation. The increase in 478-nm absorption on conversion to the homogeneous  $\text{Mn}^{3+}$  form indicates that at least 40% of the active sites contain  $\text{Mn}^{2+}$  in the purified enzyme, corroborating the EPR data. The broad, structured absorption for the  $\text{Mn}^{3+}$  site extends over the entire visible region but does not appear to extend beyond about 800 nm. This is consistent with an earlier characterization of this enzyme showing essentially base line absorption for MnSD in the near-IR region (800–1300 nm).<sup>22</sup> The distinctive features of the visible absorption spectrum for native  $\text{Mn}^{3+}$ SD are a partly resolved shoulder (the "red band", see below) near 600 nm, a well-defined notch near 485 nm, and a maximum absorption intensity at 478 nm. The minimum absorption intensity in the near-UV produces a trough near 375 nm, which is more pronounced in this sample than in earlier reports. The broad optical absorption in the visible region is clearly not a single electronic transition, and additional structure is evident in the first-derivative transformation of the absorption data, as shown in Figure 2. In the absorption derivative spectrum, the broad absorption envelope reveals both broad features with inflections near 650, 550, and 430 nm, as well as sharper features, most prominently in the region 425–575 nm but extending over the lower energy range as well.

Circular dichroism spectroscopy (Figure 3) resolves more structure than optical absorption in the visible spectrum, with at least four transitions evident in the region between 350 and 800 nm. The spectrum we observe is similar to data previously reported for MnSD,<sup>21</sup> but we find no evidence for additional CD features beyond 600 nm, and there are also differences in the near-UV

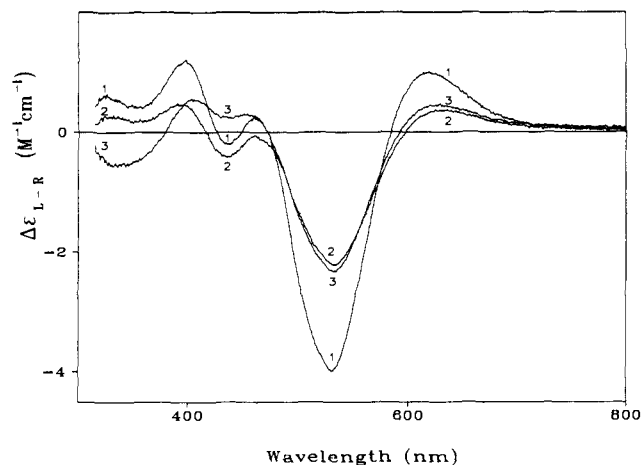


**Figure 3.** Circular dichroism spectra of  $\text{Mn}^{3+}$  superoxide dimutase and derivatives.  $\text{Mn}^{3+}$ SD (1 mM active sites), in 50 mM potassium phosphate buffer (pH 7.0): 1, native; 2, in the presence of 400 mM KF; 3, in the presence of 80 mM  $\text{KN}_3$ .

region. The strongest CD is associated with a transition near 550 nm, in a region lacking any resolved absorption band. This spectral feature is clearly resolved from the red band, which appears as a lower energy shoulder in absorption, but has oppositely signed intensity in CD. The red band occurs in the native enzyme near 600 nm, and no additional CD features are observed to lower energy. At least two poorly resolved features contribute to the CD spectrum between 375 and 460 nm, the most prominent feature being a maximum in CD at 400 nm.

The application of a longitudinal magnetic field turns on MCD selection rules, and field- and temperature-dependent MCD intensity will in general be expected for a paramagnetic metal complex. For  $\text{Mn}^{3+}$ SD, we observe temperature-dependent C-term MCD intensity associated with the visible absorption features. The strongest MCD intensity occurs in two transitions, giving rise to a pair of MCD bands at 470 and 593 nm, of oppositely signed but nearly equal intensity, with a sharp positive MCD feature on the low-energy side of the 470-nm band. These MCD signals are sensitive to varying magnetic field and temperature, and separate field and temperature profiles for the MCD spectra are shown in Figure 4 to emphasize the distinctive characteristics found for each of these perturbations. The variation of MCD intensity with magnetic field strength at low, constant temperature (4.2 K) (Figure 4, bottom) shows nearly linear increase over the entire field range covered in the experiment (0–5.5 T) reflected in the nearly constant increments for the increase in MCD signal amplitude. In contrast, the temperature dependence of the MCD intensity at fixed magnetic field strength (4.0 T) exhibits a pronounced saturation effect below approximately 5 K. The saturation of MCD occurs as a deviation from Curie law ( $1/T$ ) temperature dependence, which is clearly evident when the temperature points are chosen in a reciprocal progression as in Figure 4 (top).

The information contained in the MCD saturation behavior is most directly accessible when the variation of MCD intensity is plotted as saturation magnetization curves over a wide range of temperature and magnetic field strength in terms of the saturation parameter  $\beta H/2kT$ . The saturation magnetization curves for  $\text{Mn}^{3+}$ SD shown in Figure 5 exhibit a strong nesting of curves, and even at the lowest temperature (1.7 K) field saturation is not completely achieved by the high-field (5.5 T) limit. All of these MCD experiments on the oxidized SD are complicated slightly by the observation that the active site  $\text{Mn}^{3+}$  is reduced slowly on standing in buffered 50% glycerol typically used as the glassing solvent for low-temperature optical studies. At room temperature, we find that the rate of reduction is less than 1%/min, so the extent of reduction can be made negligible by rapidly adding the glycerol to the sample and freezing it immediately in the cryostat. No spontaneous reduction occurs for the oxidized enzyme in the absence of glycerol over several hours.

(25) Lawrence, G. D.; Sawyer, D. T. *Biochemistry* 1979, 14, 3045–3050.

(26) Sato, S.; Nakazawa, K. *J. Biol. Chem.* 1978, 83, 1165–1171.

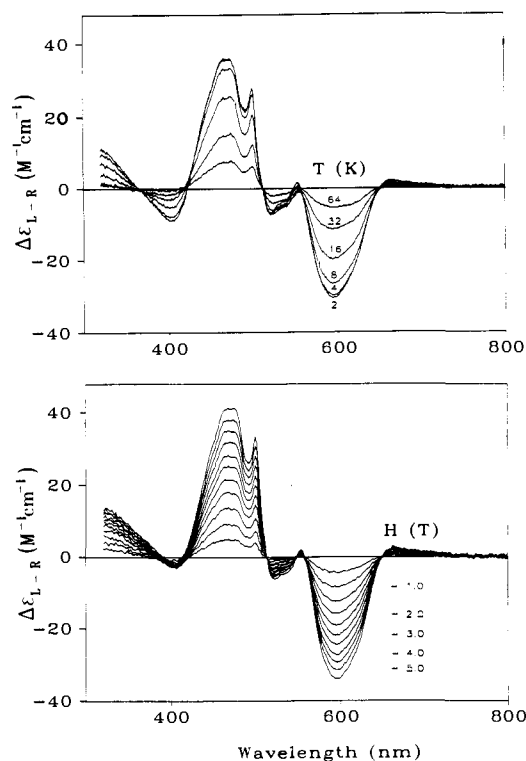


**Figure 4.** MCD spectra for  $\text{Mn}^{3+}$  superoxide dismutase.  $\text{Mn}^{3+}\text{SD}$  (1.6 mM active sites) in 50% glycerol, 25 mM potassium phosphate buffer (pH 7.0): top, variable-temperature MCD recorded at magnetic field strength of 4.0 T; bottom, variable magnetic field MCD at constant temperature (4.2 K).

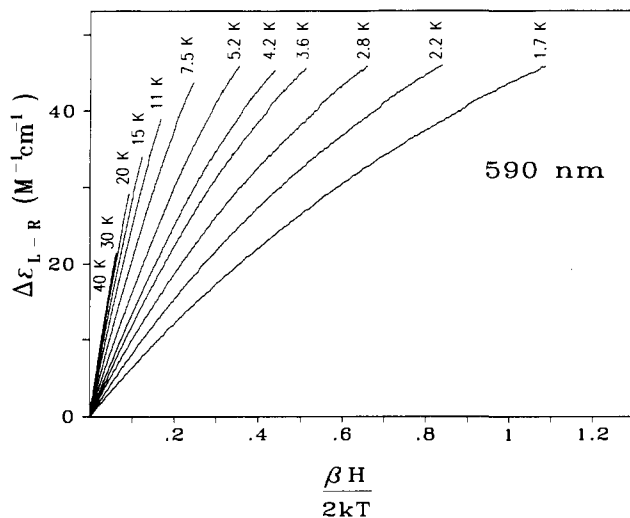


**Figure 5.** Saturation magnetization curves for  $\text{Mn}^{3+}$  superoxide dismutase. Data recorded at 590 nm for temperature range from 1.7 to 40 K and magnetic field strength from 0 to 5.5 T.

In low-temperature X-band EPR experiments, no spectroscopic features arising from the  $\text{Mn}^{3+}$  site are detected in the field range 25–5000 G.

**B. Ligand Interactions.** Addition of anions ( $\text{F}^-$ ,  $\text{N}_3^-$ ) to  $\text{Mn}^{3+}\text{SD}$  results in a perturbation of each of these spectra as shown in Figures 1, 2, 3, 7, and 8. The absorption spectra decrease in intensity by approximately 30% ( $\epsilon_{449}^{\text{Mn}} = 560 \text{ M}^{-1} \text{ cm}^{-1}$  for  $\text{Mn}^{3+}\text{SD}-\text{N}_3^-$ ), and the absorption maximum shifts to higher energy (to 461 nm ( $\text{F}^-$ ) and 449 nm ( $\text{N}_3^-$ )) in the ligand complexes. Absorption derivative spectra for the two complexes (Figure 2) permit additional structure to be detected in the visible absorption band, including a pattern of sharp features near 500 nm. The progress of the titration of the active site by anions can be conveniently monitored by following the changes in absorption intensity, and Figure 6 shows the experimental data and calculated

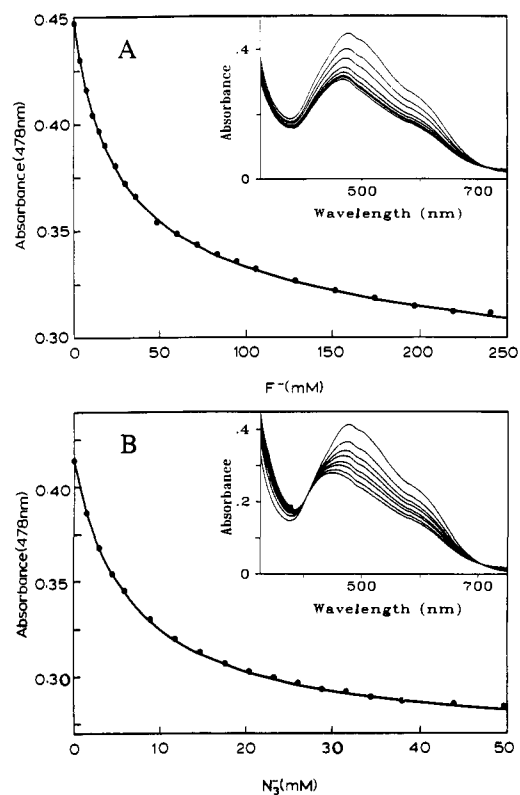


**Figure 6.** Optical titration of  $\text{Mn}^{3+}$  superoxide dismutase with A, KF (0.26 mM enzyme) in 50 mM potassium phosphate buffer, pH 7.0; B,  $\text{KN}_3$  (0.24 mM enzyme) in 50 mM potassium phosphate buffer, pH 7.0; (●) experimental data; (—) calculated as described in the text.

binding isotherms for  $\text{F}^-$  and  $\text{N}_3^-$  complex formation. For the  $\text{N}_3^-$  titration, a single isosbestic point is observed at 408 nm between the spectra of the native enzyme and the anion complex. Dissociation constants for both of these complexes have been extracted from the experimental data by nonlinear regression against an equilibrium binding model,<sup>27</sup> yielding  $K_D$  values of 25 mM and 1.1 M for two-step binding of  $\text{F}^-$  and 7.2 mM for single-step  $\text{N}_3^-$  complexation. Attempts to account for the absorbance changes observed during the  $\text{F}^-$  titration with a single-step binding reaction led to a much poorer agreement between experiment and theory, whereas a single-step binding isotherm provides an adequate fit for the  $\text{N}_3^-$  titration. CD spectra of the  $\text{F}^-$  and  $\text{N}_3^-$  complexes (Figure 3), like the absorption spectra, exhibit a decrease in intensity but no dramatic change in structure compared to the corresponding spectra of native  $\text{MnSD}$ . The CD spectra of the two complexes are nearly superimposable over the spectral range 420–800 nm, and the approximately 40% decrease in intensity compared to the CD spectrum of the unliganded native  $\text{Mn}^{3+}\text{SD}$  parallels the similar decrease in the intensity of the absorption spectra.

While both absorption and CD spectra of the anion complexes closely resemble the corresponding spectra of the unliganded protein, there are dramatic differences in the MCD spectra (Figure 7 and 8). Both complexes exhibit temperature-dependent C-terms in MCD, but in contrast to the unliganded protein, the strongest C-term intensity for the  $\text{F}^-$  and  $\text{N}_3^-$  adducts of  $\text{Mn}^{3+}\text{SD}$  is associated with the highest energy visible absorption and CD features and appears as a pair of MCD features of nearly equal but oppositely signed intensity forming a pseudo-A-term centered at 435 nm, with positive MCD in the lower energy component. MCD spectra for the two anion complexes are very similar, but the  $\text{F}^-$  adduct is distinguished by the appearance of partly resolved structure in the lower energy band. The fluoride concentration for this sample was chosen on the basis of titration data to give an average of one anion bound per active site, which results in

(27) Slykhouse, T. O.; Fee, J. A. *J. Biol. Chem.* **1976**, *251*, 5472–5477.

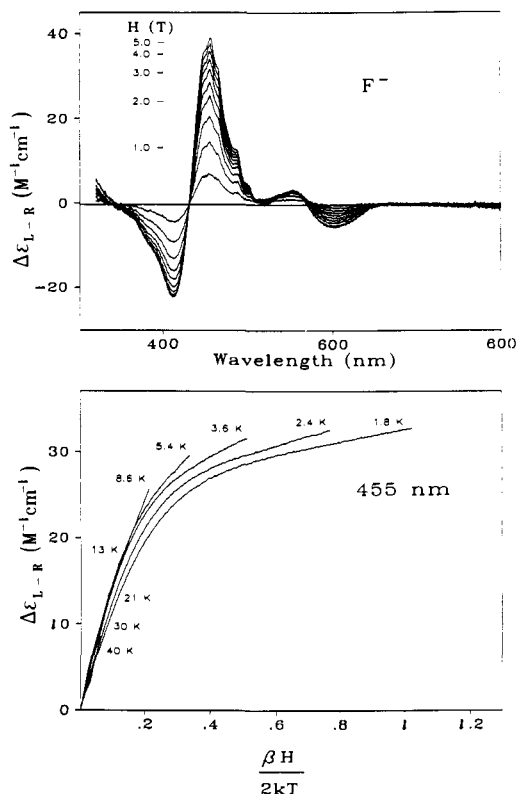


**Figure 7.** MCD spectra for fluoride complex of  $\text{Mn}^{3+}$  superoxide dismutase.  $\text{Mn}^{3+}\text{SD}$  (2.0 mM active sites) in 50% glycerol, 25 mM potassium phosphate buffer (pH 7.0) containing 200 mM KF: top, variable magnetic field MCD recorded at 4.5 K; bottom, saturation magnetization curves recorded at 455 nm for low-temperature, variable magnetic field MCD over a range of temperatures from 1.8 to 40 K and magnetic fields to 5.5 T.

the presence of small fractions of unliganded and dianion complexes in addition to the monoanion complex majority species. The weak MCD near 590 nm in this sample appears to arise from the approximately 5% unliganded sites and is eliminated at a higher fluoride concentration. A sharp feature occurs in the MCD spectra for both of these complexes near 540 nm with low intensity. The magnetic field dependence of the MCD spectra for these two complexes is illustrated in the series of spectra shown at the top of Figures 7 and 8 and is very different from that found for the unliganded protein. There is a clear deviation from linear dependence of signal amplitude on magnetic field strength, and the marked approach to saturation of MCD intensity at the highest field distinguishes the anion complexes. This approach to saturation of MCD is particularly evident in the saturation magnetization curves (Figures 7 and 8, bottom), which also convey the relatively small nesting associated with the MCD magnetization curves obtained over a wide temperature range.

As found for the native  $\text{Mn}^{3+}\text{SD}$ , the anion complexes exhibit no detectable EPR signals at X-band in the magnetic field range from 50 to 5000 G.

MCD data were recorded for a five-coordinate mononuclear  $\text{Mn}^{3+}$  complex, manganese pentachloride  $[\text{Et}_4\text{N}]_2[\text{MnCl}_5]$ ,<sup>18</sup> as shown in Figure 9 (top). MCD C-term intensity is observed in two pseudo-A-term features centered at 425 and 632 nm. The 1.8-K MCD saturation magnetization curve for this complex is shown in Figure 9 (bottom). No MCD intensity is observed to lower energy in the 750–1000-nm range at high magnetic field (5.0 T) and low temperature (4.5 K).

**Manganous ( $\text{Mn}^{2+}$ ) Superoxide Dismutase.** On reduction of  $\text{MnSD}$  with sodium dithionite, the purple color of the oxidized enzyme is lost and a colorless solution is obtained. However, the Mn remains bound in the protein, with no significant change in metal content following reduction and desalting. Reduction also has no effect on the specific activity of the purified enzyme.  $\text{Mn}^{2+}\text{SD}$  spontaneously reoxidizes in air to give a mixture of  $\text{Mn}^{2+}$

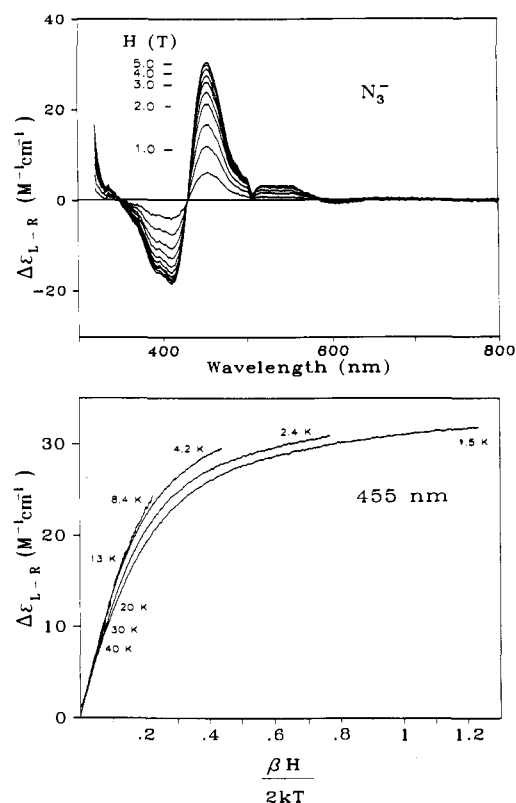


**Figure 8.** MCD spectra for azide complex of  $\text{Mn}^{3+}$  superoxide dismutase.  $\text{Mn}^{3+}\text{SD}$  (2.0 mM active sites) in 50% glycerol, 25 mM potassium phosphate buffer (pH 7.0) containing 80 mM  $\text{KN}_3$ : top, variable magnetic field MCD spectra recorded at 4.5 K; bottom, MCD saturation magnetization curves recorded at 455 nm for low temperature (1.5–40 K), over a variable magnetic field range (to 5.5 T).

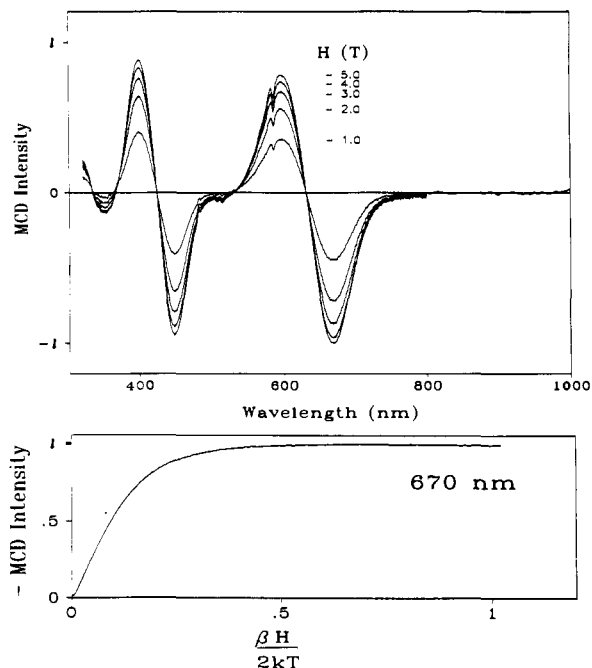


**Figure 9.** MCD data for manganese pentachloride  $[\text{Et}_4\text{N}]_2[\text{MnCl}_5]$ : top, low-temperature (1.8 K) MCD spectra for a mulled sample over a magnetic field range from 1 to 5 T, only the 5 T MCD spectrum recorded in the range 800–1000 nm; bottom, MCD magnetization curve for manganese pentachloride recorded at 670 nm (temperature, 1.8 K; magnetic field strength, 0–5 T).

and  $\text{Mn}^{3+}$  forms, partly restoring the purple color of the native enzyme. No absorption is observed for  $\text{Mn}^{2+}\text{SD}$  over the UV-visible spectral range below the protein absorption cutoff near 300 nm, and even at 7.5 mM active sites and 1-cm light path, no CD

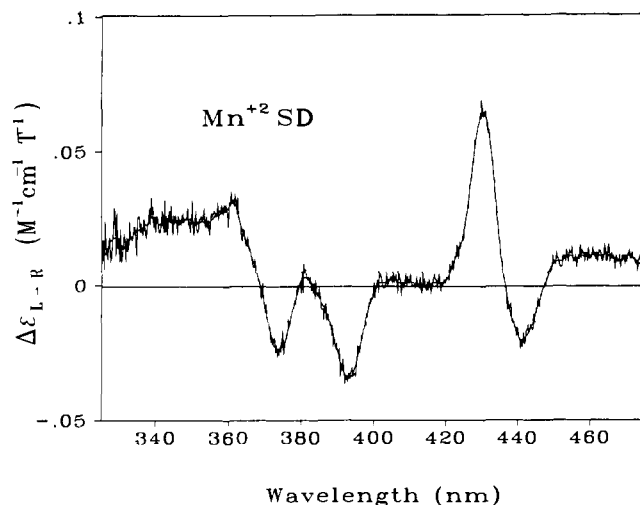


**Figure 10.** Low-temperature MCD for  $\text{Mn}^{2+}$  superoxide dismutase. Anaerobic MnSD (7.5 mM active sites) in 50% glycerol, 25 mM potassium phosphate buffer (pH 7.0) reduced with a slight excess of dithionite (temperature, 1.8 K; magnetic field strength, 5.5 T).

signals have been detectable at room temperature. In MCD spectra at low temperatures, however, relatively weak but sharp and well-defined spectra emerge over this spectral range, as shown in Figure 10. These features are dominated by a multiplet of signals near 375, 390, and 430 nm. To rule out the possibility that these signals derive from free  $\text{Mn}^{2+}$  in solution, we have recorded spectra of a 50% glycerol glass containing 2 mM  $\text{Mn}^{2+}\text{SO}_4$  under identical conditions of temperature and magnetic field, which exhibit no detectable MCD intensity. We have checked for free manganese in the  $\text{Mn}^{2+}\text{SD}$  MCD sample in a separate experiment by desalting the reduced protein and find that there was virtually no loss of Mn from the active site, indicating that at least the majority of  $\text{Mn}^{2+}$  remained bound to the protein under these conditions.

The helium temperature X-band EPR spectra of reduced MnSD species are shown in Figure 11. Extremely complex resonance behavior is observed over the entire magnetic field range of the experiment for all three of these samples. The reduced native enzyme exhibits a spectrum (Figure 11, top) similar to that previously reported for this form,<sup>22</sup> characterized by transitions between 500 and 2250 G. Broad signals are also present at higher field, extending to at least 15 000 G. Mn metal hyperfine structure can be partly resolved in the spectrum of the unliganded  $\text{Mn}^{2+}\text{SD}$ , where a sextet splitting with  $a_{\text{Mn}} = 85$  G is observed in the  $g = 5.80$  feature. The sharp features near  $g = 2$  in this spectrum are the six-line EPR spectrum from a small amount of free  $\text{Mn}^{2+}$  impurity in this sample. Addition of anions to the solution of reduced protein results in a major perturbation of the EPR spectrum, with distinctly different spectra for  $\text{F}^-$  and  $\text{N}_3^-$  complexes. The fluoride complex is similar in appearance to the native enzyme, although the Mn hyperfine structure is not resolved and some intensity appears in the low-field region below 500 G. Addition of azide even more dramatically perturbs the  $\text{Mn}^{2+}$  center, leading to appearance of an unusual EPR spectrum with intensity increasing toward zero field, continuous absorption to approximately 4000 G, and reduced intensity in features to higher field.

### Discussion

Manganese metalloenzymes are emerging as a diverse group of proteins with biological functions ranging from guanidinium group hydrolysis in arginase<sup>28,29</sup> to the well-known water-splitting chemistry of the photosynthetic reaction center.<sup>2</sup> In addition to these catalytic Mn complexes, there are a number of proteins in which bound manganese (as  $\text{Mn}^{2+}$ ) appears to have a structural

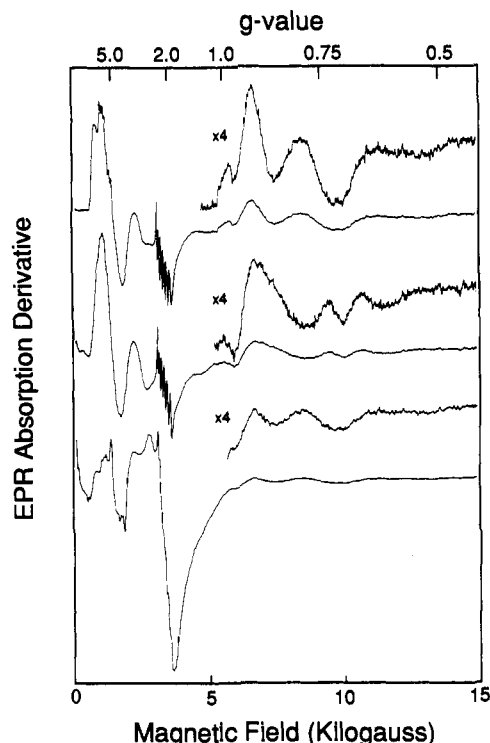


**Figure 11.** EPR spectra for  $\text{Mn}^{2+}$  superoxide dismutase: top, anaerobic solution of MnSD (3.3 mM active sites) reduced with dithionite under argon; middle, solution of  $\text{Mn}^{2+}\text{SD}$  (3.0 mM active sites) containing 1 M KF; bottom, solution of  $\text{Mn}^{2+}\text{SD}$  (2.8 mM active sites) containing 1 M  $\text{KN}_3$ . The spectrum of an appropriate anaerobic buffer blank subtracted from the data for each of the protein complexes. Instrumental parameters: temperature, 5 K; microwave frequency, 9.46 GHz; microwave power, 1 mW; modulation amplitude, 10 G.

role comparable to that found for other divalent cations such as  $\text{Mg}^{2+}$  or  $\text{Ca}^{2+}$  with which it is sometimes associated.<sup>1</sup> In contrast to the relatively well studied Fe and Cu sites in proteins, all of these Mn complexes are just beginning to be characterized in detail. The manganese site in MnSD is particularly attractive as a starting point for detailed spectroscopic characterization of biological Mn complexes because it has a relatively simple mononuclear coordination structure now defined by crystallographic studies,<sup>9,10</sup> is available in reasonable quantities from biological sources, and can be prepared in two distinct redox forms relating to its catalytic activity. Our initial focus in Mn bioinorganic spectroscopy has therefore been strongly directed at MnSD with the expectation that this site will provide a basis for extension of this work to Mn sites in other proteins with Mn clusters and perhaps more complex active site interactions.

In addition to the intrinsic interest of biological Mn complexes, strong parallels appear to exist between the bioinorganic chemistry of Mn and Fe. There are a number of examples of the isolation of functionally or even structurally homologous enzymes having either Mn or Fe in their active sites, including superoxide dismutase, ribonucleotide reductase,<sup>30,31</sup> and phenolytic dioxygenases.<sup>32</sup> For superoxide dismutase, the parallel is further strengthened by the observation that, in some cases, the same apoenzyme can bind either Mn or Fe to form an active complex.<sup>33</sup> Results of studies on MnSD may therefore directly relate to the corresponding Fe site in FeSD.

The developing studies on Mn sites in proteins require working (effective) probes of the environment and interactions of the active

(30) Atkin, C. L.; Thelander, L.; Reichard, P.; Lang, G. *J. Biol. Chem.* **1973**, *248*, 7464-7472.

(31) Willing, A.; Follmann, H.; Auling, G. *Eur. J. Biochem.* **1988**, *170*, 603-611.

(32) Que, L., Jr.; Widom, J.; Crawford, R. L. *J. Biol. Chem.* **1981**, *256*, 10941-10944.

(33) Amano, A.; Shizukuishi, S.; Tsunemitsu, A.; Maekawa, K.; Tsunawana, S. *FEBS Lett.* **1990**, *272*, 217-220.

(28) Harell, D.; Sokolovsky, M. *Eur. J. Biochem.* **1972**, *25*, 102-108.

(29) Ganadu, M. L.; Pinna, G. G.; Sisini, A.; Scozzafava, A. *Inorg. Chim. Acta* **1984**, *92*, 9-14.

site metal ion. X-ray crystallographic methods are the ultimate tool for obtaining geometric structures for biological complexes at nearly atomic resolution but have little to say regarding the electronic features that are important for chemistry. Spectroscopy, on the other hand, can provide information at this electronic structural level of resolution, giving insight into electronic wave functions and energy splittings that enter into the molecular interactions of the active site in catalysis. We are particularly interested in exploring the information contained in absorption, CD, MCD, and EPR spectra for  $Mn^{2+}$  and  $Mn^{3+}$  centers in proteins, beginning with the relatively simple case of MnSD. This analysis will establish effective probes of Mn sites in proteins and discuss the basic information contained in the spectroscopic data.

**Ligand Field Theory Background.  $Mn^{3+}$  Complexes.** The  $Mn^{3+}$  ion has a  $3d^4$  electronic configuration that is one electron short of a half-filled shell, so that four of the five d-orbitals will be half-occupied in a high-spin complex.<sup>34-37</sup> The consequence of this in the electronic structure and spectroscopy of  $Mn^{3+}$  complexes is that ligand field states may be conveniently labeled as hole states, with electronic symmetry labels defined by the symmetry of the unfilled d-orbital. The spectroscopically important low-energy ligand field excited states, differing in the spatial localization of the hole within the d-orbital set, are correspondingly defined by the symmetry of the vacant orbital, making this labeling scheme the basis for describing ligand field spectra.

Metal-ligand interactions in transition ion complexes result in splittings within the 3d orbital set that most sensitively reflects the angular features of coordination geometry. Simple one-electron ligand field calculations<sup>38</sup> can give a qualitative picture of metal d-orbital splittings and so provide a conceptual link between spectroscopic data and the structural features of a coordination complex. This is especially true for a one-electron or one-hole metal ion ( $d^{1,4,6,9}$ ) where there is a direct correspondence between orbital configurations and electronic states. This approach is particularly valuable when an idealized or limiting effective symmetry may be assigned to the complex, making it possible to evaluate selection rules for spectroscopic transitions, thus providing the basis for a more detailed interpretation of spectra. One limitation of this approach is that it restricts itself to consideration of d-shell electronic configurations, neglecting charge transfer excited states that may contribute significantly to the ligand field spectra (both intensities and energy splittings) through covalency.<sup>34,37</sup> While the ligand field approach retains its value as a simple description of metal ion electronic structure in complexes, these limitations may lead to behavior not predicted within the restricted ligand field picture.

The active site manganese in MnSD is known from crystallographic studies<sup>9,10</sup> to be five-coordinate with roughly trigonal-bipyramidal (TBP) or square-pyramidal (SP) geometry, the precise bond angles being uncertain at the current level of crystallographic resolution. In the course of the following analysis, there will be occasion to consider both of these limits for the coordination environment, with the Berry pseudorotation coordinate<sup>39,40</sup> ( $C_{2v}$  distortion) providing a connection between the two limits. The  $C_{2v}$  site symmetry will prove sufficiently general to consider in both trigonal-bipyramidal ( $D_{3h}$ ) and square-pyramidal ( $C_{4v}$ ) limits, so the analysis will often be referred to this case. While the actual site symmetry for  $Mn^{3+}$  in the protein cannot be higher than  $C_1$ , the choice of a higher effective site symmetry can be justified by the significant insight it provides into the

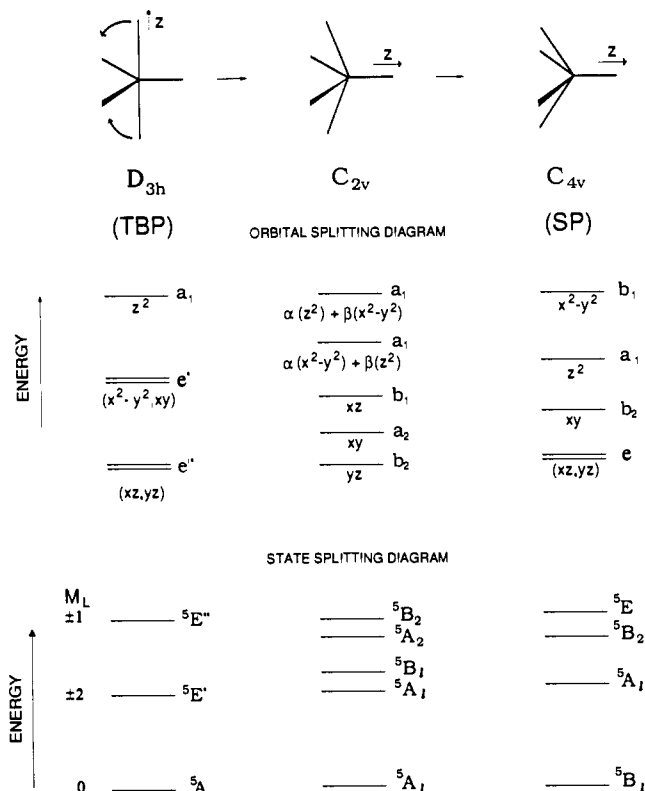


**Figure 12.** Correlation diagram for orbital and electronic state splittings for a five-coordinate  $Mn^{3+}$  complex under the  $C_{2v}$  distortion coordinate between trigonal-bipyramidal (TBP) and square-pyramidal (SP) limiting geometries.

spectroscopic data. Figure 12 shows a qualitative ligand field d-orbital splittings diagram for the transformation of a trigonal bipyramid into a square pyramid via an intermediate  $C_{2v}$  site symmetry. In the  $D_{3h}$  limit, the d-orbitals split into two doublets and a singlet, with the orbitally nondegenerate singlet at highest energy, destabilized by the axial interactions along  $z$ , the  $z$  axis being chosen along the trigonal axis in this limit (Figure 12, top). Filling these orbitals with four d-electrons defines the orbital ground-state configuration  $(e'')^2(e')$ , leaving the nondegenerate  $a_1$  orbital ( $d_{z^2}$ ) empty. As indicated earlier, the electronic states for a high-spin  $d^4$  metal complex derive their symmetry labels from the unfilled orbital, and the trigonal-bipyramidal  $Mn^{3+}$  complex is thus predicted to have a  $d_{z^2}$  orbital ground state ( $A_1$  symmetry; Figure 12, bottom). Two orbitally degenerate ligand field excited states ( $E'$  and  $E''$  symmetries in  $D_{3h}$ , represented respectively by the degenerate orbital combinations  $(d_{xz}, d_{yz})$  and  $(d_{x^2-y^2}, d_{xy})$ ) occur at higher energy. The orbital degeneracies in these states derive from the  $M_L = \pm 1$  and  $\pm 2$  spherical components of the d-orbital wave functions, and thus these states contain unquenched orbital angular momentum.<sup>37</sup> For the weak axial interaction indicated in Figure 12, the  $M_L = \pm 2$  orbital doublet lies lower in energy.<sup>38</sup>

A relabeling of coordinate axes is required in the transformation between trigonal and square-pyramidal geometries shown in Figure 12, with the axial ligands in the trigonal-bipyramidal complex assuming equatorial positions in the square pyramid.<sup>41,42</sup> This axis interchange occurs because both trigonal-bipyramidal and square-pyramidal limiting geometries represent (distinct) axial extensions of the rhombic  $C_{2v}$  structure, requiring a reorientation of the principal axis ( $z$  axis) from a 3-fold to a 4-fold axis on changing from the trigonal to the square limit. This complication is most easily dealt with by defining the axes as shown and transforming the orbital labels by the cyclic substitution  $z \rightarrow x$ ,  $x \rightarrow y$ ,  $y \rightarrow z$ , which leads to redefinition of  $d_{xz}$  as  $d_{xy}$  in the new coordinate system. Choosing the 2-fold axis as the unique axis

(34) Ballhausen, C. J. *Introduction to Ligand Field Theory*; McGraw-Hill: San Francisco, 1962.

(35) Figgis, B. N. *Introduction to Ligand Fields*; Interscience: New York, 1966.

(36) Griffith, J. S. *Theory of Transition-Metal Ions*; Cambridge University Press: Cambridge, 1964.

(37) Lever, A. B. P. *Inorganic Electronic Spectroscopy*, 2nd ed.; Elsevier: New York, 1984.

(38) Companion, A. L.; Komarynsky, M. A. *J. Chem. Educ.* **1964**, *41*, 257-262.

(39) Berry, R. S. *Rev. Mod. Phys.* **1960**, *32*, 447-454.

(40) Muertterties, E. L.; Guggenberger, L. J. *J. Am. Chem. Soc.* **1974**, *96*, 1748-1756.

(41) Rossi, A. R.; Hoffmann, R. *Inorg. Chem.* **1975**, *14*, 365-374.

(42) Hay, P. J. *J. Am. Chem. Soc.* **1978**, *100*, 2411-2417.

( $z$  axis) to correlate with  $C_{2v}$  symmetry results in the assignment of  $d_{xy}$  and  $d_{x^2-y^2}$  to different orbital doublets. Reference to group theory representation tables shows that a rotation about  $z$  (corresponding to a matrix element of  $L_z$ ) spans these two orbitals in  $C_{2v}$  symmetry, indicating that spin-orbit coupling will be effective in mixing these levels. As will become apparent below, this has important consequences for MCD spectroscopy in a distorted trigonal complex.

Lowering the symmetry completely lifts the orbital degeneracies and leads to mixing between  $d_{x^2-y^2}$  and  $d_{z^2}$  orbital wave functions, which both transform with  $a_1$  symmetry in the  $C_{2v}$  symmetry point group. Correlating between the two limiting geometries in Figure 12, the ground state (defined by the highest lying orbital in the upper scheme) changes from predominantly  $d_{z^2}$  character in the trigonal-bipyramidal limit to predominantly  $d_{x^2-y^2}$  in the square-pyramidal limit. This is represented by labeling the orbital as a linear combination,  $\alpha(d_{z^2}) + \beta(d_{x^2-y^2})$ , with the coefficients  $\alpha$  and  $\beta$  normalized to give  $\alpha^2 + \beta^2 = 1$  with  $\beta = 0$  in the trigonal limit, increasing to a value of 1 in the square-pyramidal limit. Four nondegenerate ligand field excited states are expected for the  $C_{2v}$   $Mn^{3+}$  site, within each of which orbital angular momentum is quenched. This leads to a predicted resolution of up to four separate spin-allowed ligand field transitions in the  $C_{2v}$  complex.

In the  $C_{4v}$  limit, where the ground state is defined by a  $d_{x^2-y^2}$  orbital wave function ( $B_1$  symmetry), three ligand field excited states are predicted at higher energy: two orbitally nondegenerate ( $A_1$ ,  $B_2$ ) and one orbitally degenerate ( $E$ ). The ( $xz$ ,  $yz$ ), orbital degeneracy in the  $E$  state leaves one component of orbital angular momentum unquenched ( $L_z' = 1$ ), resulting in an in-state spin-orbit coupling for the orbital doublet, which is important for MCD intensities in the  $C_{4v}$  complex. At most, three distinct  $d \rightarrow d$  transitions may occur within the square-pyramidal  $Mn^{3+}$  site, and from this simple analysis it is evident that the limiting axial complexes (either  $D_{3h}$  or  $C_{4v}$ ) can be distinguished from a rhombic structure ( $C_{2v}$ ) on the basis of the number of resolved ligand field transitions: three in either axial limit and four in lower symmetry.

Ground-state splittings arising from spin multiplicity are important for MCD and EPR spectroscopies as well as magnetic susceptibility. The high-spin configuration for a  $d^4$  metal ion, expected in the weak ligand environments of biological complexes, is a quintet ( $S = 2$ ) state, and so  $Mn^{3+}$  sites in proteins will generally have a paramagnetic ground state. Since  $Mn^{3+}$  is an integer-spin (non-Kramers) ion, the degeneracy of the spin sub-levels may be completely removed in the absence of a magnetic field by electrostatic effects, quenching angular momentum. This is described in terms of a spin Hamiltonian for the quintet ground state:<sup>43</sup>

$$H = SDS + g\beta HS \quad (1)$$

$$= D(S_z^2 - 2) + E(S_x^2 - S_y^2) + g_1\beta HS_z \cos \theta + g_2\beta HS_x \sin \theta \quad (2)$$

clearly expressing the anisotropy (orientation dependence) of the ground-state Zeeman interaction in the angular factors of the last two terms. Here,  $D$  and  $E$  are respectively the axial and rhombic zero-field splitting parameters deriving from spin-orbit coupling within the  $d$ -orbital states, leading to splitting of the 5-fold degeneracy of the ground spin multiplet as shown in Figure 13 for two axial limits. The axial zero-field splitting  $D$  splits the  $M_s$  states on the basis of the magnitude rather than the sign of  $M_s$ , leaving degenerate pairs except for  $M_s = 0$ , which remains a nondegenerate level. For the  ${}^5A_1$  ground state associated with  $Mn^{3+}$  in trigonal-bipyramidal geometry, spin-orbit coupling among the ligand field states leads to positive  $D$  ( $D > 0$ ), which can be evaluated in second-order perturbation theory as  $D = \lambda^2(3/E - ({}^5E''))$ , while the  ${}^5B_1$  ground state in square-pyramidal geometry exhibits negative zero-field splitting ( $D < 0$ ) with  $D = \lambda^2((1/E - ({}^5E)) - (4/E({}^5B)))$ . The inverted splitting scheme in the latter

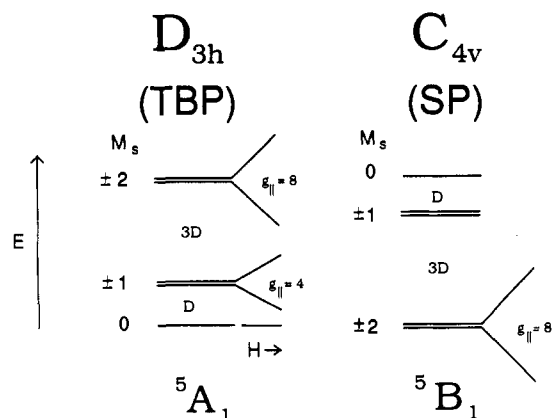


Figure 13. Ground-state splittings for trigonal-bipyramidal and square-pyramidal limiting geometries for a  $Mn^{3+}$  site.

case places a non-Kramers doublet lowest in the ground state, while a nondegenerate level is lowest for positive  $D$ . The degeneracy of the two non-Kramers doublets that are left by the axial splitting  $D$  is completely lifted in lower symmetry by the rhombic zero-field splitting term  $E$  in the spin Hamiltonian<sup>43</sup> (eq 2). For low-symmetry complexes typical of those encountered in proteins, these zero-field splittings are often larger than the microwave energy of conventional EPR instrumentation, making the ground states EPR-inaccessible.<sup>44</sup> However, the quenched paramagnetism in these complexes may still be expressed in a magnetic susceptibility or MCD experiment where the Zeeman energy can compete with the zero-field splitting and induce a magnetic moment in the ground state.

The metal  $d$ -orbital splittings described above lead to the existence of distinct ligand field excited states shown in the lower scheme in Figure 12 differing from the ground state in the distribution of metal electron density over  $3d$  orbital wave functions. Transition intensities for the  $Mn^{3+}$  ion depend on selection rules for orbital excitation that can be evaluated within the conceptual picture described above.<sup>34-37</sup> Transitions among  $d$ -orbital states will of course be parity forbidden (Laporte rule) but can occur with low intensity through relaxation of optical selection rules by mixture of odd-parity excited states into the ligand field states in low symmetry. Spin selection rules for electronic transitions result in the greatest intensity appearing in  $\Delta S = 0$  excitations, the spin-allowed spectroscopic transitions that dominate the absorption spectra. Spin-orbit coupling operates to mix orbital and spin angular momentum wave functions, relaxing the spin selection rule and making spin-forbidden spectra weakly allowed. For  $Mn^{3+}$ , the magnitude of the spin-orbit interaction is defined by the one-electron spin-orbit coupling constant<sup>34</sup>  $\xi_{Mn^{3+}, free ion} = 355 \text{ cm}^{-1}$ , which yields a many-electron spin-orbit coupling constant  $\lambda_{Mn^{3+}, free ion} = \xi/2S = 90 \text{ cm}^{-1}$ . In complexes, where this value will generally be reduced by approximately 20% by covalency, spin-orbit interactions remain a significant perturbation relative to ligand field energies and in particular are the origin of ground-state zero-field splittings, the basis for MCD intensity in low symmetries, as well as providing a mechanism for intensity in the formally forbidden quintet-triplet ( ${}^5T \rightarrow {}^3T$ ) transitions. The bandwidth of  $d \rightarrow d$  spectra of coordination complexes are typically broad, reflecting changes in geometry of the metal complex in the ligand field excited states. Unusually sharp transitions appearing in excited-state spectra are characteristic of ligand field independent transitions, which relate to excited states having the same orbital configuration as the electronic ground state and in general involve spin-forbidden transitions.

Distinct selection rules apply for each of the spectroscopic approaches (optical absorption, CD, and MCD spectroscopies), making the combination of complementary approaches more powerful in probing electronic structure of metal complexes than

(43) Abragam, A.; Bleaney, B. *Electron Paramagnetic Resonance of Transition Ions*; Oxford University Press: Oxford, 1970, pp. 209-216.

(44) Hendrich, M. P.; Debrunner, P. G. *J. Magn. Reson.* 1988, 78, 133-141.

any individual method. A brief summary of the distinct selection rules operating in each of these spectroscopies will prove useful in further discussion.<sup>34,45</sup> Intense optical absorption requires an electric dipole transition moment in an electronic transition, associated with a transition moment operator transforming like the components of a vector ( $x, y, z$ ). CD selection rules, on the other hand, require both electric and magnetic dipole components in a transition, magnetic dipole allowed transitions being associated with an orbital transition moment operator transforming like the components of space rotations ( $R_x, R_y, R_z$ ). In transition-metal complexes,  $d \rightarrow d$  transitions themselves may be magnetic dipole allowed, making it possible to predict qualitatively which transitions will dominate in CD spectra of a metal complex by evaluating the magnetic dipole selection rules over the ligand field transitions. The selection rules for MCD spectroscopy are different from those for natural CD and require orbital degeneracy (angular momentum) in either the ground or excited electronic state.<sup>45</sup> This would seem to severely limit the usefulness of MCD spectroscopy in studies of metalloenzyme active sites, since orbital degeneracies imply a high-symmetry environment for the metal ion notably lacking in the biological complexes. However, spin-orbit coupling in transition-metal complexes is a sufficiently large perturbation that even in quite low symmetry orbital states may be mixed, providing a mechanism for MCD intensity. Spin-orbit coupling in the ground state is also required to induce temperature dependence in MCD transitions, since this effect is a consequence of varying population over the spin multiplet of a paramagnetic ground state, which in the absence of spin-orbit coupling is uncoupled from the orbital selection rules from which MCD intensity derives. Saturation of MCD intensity by thermal or magnetic perturbations occurs in the limit of low temperature and large Zeeman splittings where only the lowest sublevel is appreciably populated. This sensitivity to zero-field and Zeeman splittings makes saturation magnetization studies valuable in probing paramagnetic ground states.<sup>49</sup>

#### Spectroscopy of the $Mn^{3+}$ Active Site in Superoxide Dismutase.

These ligand field theory preliminaries provide the necessary background for analyzing the spectra for  $Mn^{3+}$  complexes of SD. The absorption spectrum of the unliganded native enzyme consists of a broad absorption band in the visible region of the spectrum with no evidence of significant absorption to lower energy. The intensity for this absorption ( $\epsilon_{478} = 1650 \text{ M}^{-1} \text{ cm}^{-1}$  for the dimeric protein, yielding  $\epsilon^{Mn} = 850 \text{ M}^{-1} \text{ cm}^{-1}$  per active site) is characteristic of spin-allowed ligand field spectra for a high-spin  $Mn^{3+}$  ion.<sup>19,37</sup> The intensity of the visible absorption is more than 5 times higher than that typically found for six-coordinate, roughly octahedral  $Mn^{3+}$  complexes,<sup>37</sup> where Laporte (parity) selection rules are active, and is in the range for five-coordinate  $Mn^{3+}$ . On the basis of its magnitude, the intensity found for  $Mn^{3+}$ SD can not be entirely of ligand field origin, indicating that a pure ligand field analysis of intensity information in absorption, CD, and MCD will necessarily be incomplete.

The lowest energy band in the ligand field spectra of  $Mn^{3+}$  complexes, historically called the red band, is known to provide information on coordination number based on extensive model studies that are a part of the classical ligand field theory literature.<sup>19,46-48</sup> For six-coordinate complexes, the red band occurs as a resolved transition in the near-IR region of the spectrum (800–2000 nm) and the observation that the lowest energy transition for  $Mn^{3+}$ SD is at 600 nm (absorption, CD, and MCD) is consistent with the crystallographically defined five-coordination for this site. In  $C_{2v}$  site symmetry, the red band can be assigned as the  $A_1 \rightarrow A_1$  transition between orbital states of mixed  $d_{z^2}$  and  $d_{x^2-y^2}$  character (Figure 12). Aside from the shoulder near 600 nm arising from the red band transition, the resolution of the broad absorption spectrum is insufficient to provide the basis for a ligand field analysis. Even the first-derivative absorption spectrum, where

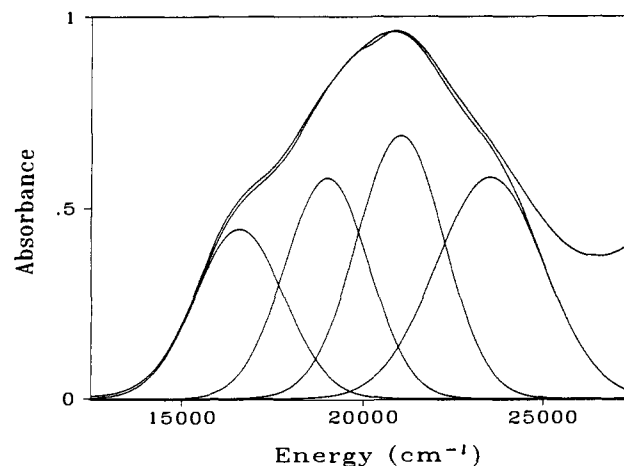


Figure 14. Gaussian resolution of spectral components in the energy spectrum of native  $Mn^{3+}$  superoxide dismutase. Transition energies estimated from resolved features in the CD and MCD spectra.

more spectroscopic detail is revealed, is inadequate for this purpose. The CD spectrum (Figure 3) provides important information in the appearance of an unusually strong CD band near 530 nm, a region not distinguished by a resolved absorption feature in the optical spectrum. This spectral feature is clearly distinct from the red band at lower energy and must derive from a second ligand field transition. Of the four spin-allowed ligand field transitions for  $Mn^{3+}$  in  $C_{2v}$  site symmetry, all but  $A_1 \rightarrow A_1$  ( $d_{z^2} \rightarrow d_{x^2-y^2}$ , the red band) are expected to have intensity in CD on the basis of magnetic dipole selection rules, with transition moment vectors transforming like  $R_x$  ( $d_{z^2} \rightarrow d_{yz}$ ),  $R_y$  ( $d_{z^2} \rightarrow d_{xz}$ ), or  $R_z$  ( $d_{z^2} \rightarrow d_{xy}$ ). A reasonable initial assignment of the second transition to the  $d_{z^2} \rightarrow d_{xz}$  orbital transition in  $C_{2v}$  symmetry ( $A_1 \rightarrow B_2$ ) is consistent with the relatively large magnetic dipole contribution expected in its transition moment. The observation that the CD intensity in this feature is large compared to the transitions at higher energy suggests possible contributions from non ligand field factors in determining these relative intensities. At least two spectral features occur in CD at higher energy with relatively lower anisotropy ( $\Delta\epsilon/\epsilon$ ) that can be identified with components of  $d_{z^2} \rightarrow d_{xy,yz}$  in  $C_{2v}$  site symmetry. The relatively small CD in these bands may be at least partly the result of partial cancellation of CD for the overlapping transitions at highest energy. In MCD, temperature-dependent C-term intensity appears mainly in two bands centered near 490 and 600 nm. The lower energy band evidently derives from the red band observed in absorption and CD, but the higher energy band lies above the region of the strong CD transition and must represent a resolved  $d \rightarrow d$  transition corresponding to the maximum of absorption intensity. The resolved ligand field spectrum in CD and particularly the pattern of MCD intensity strongly suggests a symmetry lower than axial for the  $Mn^{3+}$  site in SD. The resolution of ligand field spectral features in CD and MCD spectra of  $Mn^{3+}$ SD was used as the basis of a Gaussian deconvolution of the absorption spectrum shown in Figure 14. The energy spectrum shown in this figure covers the visible region, over which range the absorption envelope can be closely reproduced as a sum of four Gaussian bands centered at transition energies estimated from the CD and MCD spectra. This supports a low-symmetry assignment for the active site  $Mn^{3+}$  complex and illustrates how the complex absorption band shape observed for this  $Mn^{3+}$  site may arise by overlap of simpler components.

The temperature-dependent (C-term) MCD intensity we observe for  $Mn^{3+}$ SD is a consequence of thermal population over zero-field and Zeeman-split sublevels and provides a probe of the electronic ground state<sup>49</sup> of the  $Mn^{3+}$  site. Since the observed MCD increases in intensity to the lowest accessible temperature

(45) Piepho, S. B.; Schatz, P. N. *Group Theory in Spectroscopy with Applications to Magnetic Circular Dichroism*; Wiley: New York, 1983.

(46) Dingle, R. *Inorg. Chem.* **1965**, *4*, 1287–1290.

(47) Dingle, R. *Acta Chem. Scand.* **1966**, *20*, 33–44.

(48) Dingle, R. *J. Mol. Spectrosc.* **1962**, *9*, 426–427.

(49) Schatz, P. N.; Mowery, R. L.; Krausz, E. R. *Mol. Phys.* **1978**, *35*, 1537–1557.

(1.7 K), these signals must originate in the lowest sublevel of the ground state. A dramatic saturation of MCD occurs for  $\text{Mn}^{3+}\text{SD}$  at low temperature (Figure 4, top), reflecting a relatively large initial splitting among the ground-state sublevels. The optical spectra require a high-spin (quintet,  $S = 2$ ) paramagnetic ground state, yet we find only a weak magnetic field saturation effect for the MCD signal, much smaller than is typically associated with C-term MCD intensity originating within a ground state with spin degeneracies. The observed magnetic field effects are even smaller than those observed for a rhombically split non-Kramers doublet lying lowest in the ground state in the  $D < 0$  case (Figure 13, right). The results observed here suggest a positive zero-field splitting ( $D > 0$ ) term in the spin Hamiltonian for the  $\text{Mn}^{3+}$  quintet ground state, illustrated in the splitting scheme on the left in Figure 13. The dramatic nesting effect displayed by the saturation magnetization data for  $\text{Mn}^{3+}\text{SD}$  (Figure 5) is consistent with this analysis. Nesting of saturation magnetization curves reflects changes in MCD arising from a combination of thermal population and Zeeman mixing over the ground state.<sup>49</sup> For an isolated Kramers doublet ground state, the saturation curves obtained at different temperatures all overlap and no nesting occurs. For a near-degenerate non-Kramers ground doublet, only a small nesting is expressed, and even this vanishes if the doublet levels are degenerate in zero field. The degree of nesting displayed in Figure 5 reflects initial splittings that are large compared to the Zeeman terms, which are effective in mixing sublevels, and is characteristic of a ground state with positive zero-field splitting ( $D > 0$ , Figure 13, left). Magnetic susceptibility data reported<sup>22</sup> for a mixture of  $\text{Mn}^{2+}/^{3+}\text{SD}$  has been interpreted in terms of a moderate ground-state splitting  $|D| = 1\text{--}2 \text{ cm}^{-1}$ , consistent with the saturation MCD data we present here. The sign of the zero-field splitting has a geometric significance, as mentioned earlier. Positive zero-field splitting in the ground state occurs in the  $D_{3h}$  (trigonal-bipyramidal) limit of the Berry coordinate through spin-orbit coupling over the ligand field states. In this limit, the ground and first excited state (both  $A_1$  symmetry) are of mixed  $d_{x^2-y^2}$  and  $d_{z^2}$  character, with the  $d_{z^2}$  component dominating as pure trigonal axial symmetry is approached. The first and third ligand field excited states acquire predominantly  $d_{x^2-y^2}$  and  $d_{xy}$  character, respectively, in this limit (Figure 12). The MCD saturation data presented in Figures 4 and 5 thus defines the basic features of the ground-state zero-field splitting that are important for the origins of MCD intensity. By extending the analysis to excited states, we can obtain insight into the origins of the strikingly simple pattern of MCD intensity over the ligand field spectra and its structural interpretation.

The ligand field model for the  $\text{Mn}^{3+}$  active site provides the key to a deeper insight into this striking pattern of MCD intensity when selection rules for MCD are considered in more detail. The positive zero-field splitting indicated by saturation MCD data will leave a nondegenerate  $M_S$  sublevel lowest in the ground state that, in the axial limit ( $E = 0$ ), can be identified with a pure  $M_S = 0$  state. Clearly, this level cannot by itself be the origin of C-term MCD intensity but can contribute to MCD intensity through unequal admixture of components of the  $M_S = \pm 1$  doublet into  $M_S = 0$  in a magnetic field via perpendicular Zeeman ( $g_x, g_y$ ) mixing terms from eq 2. This perpendicular Zeeman mixing mechanism, which is effective in inducing MCD intensity for a  $d_{z^2}$  ground state with positive zero-field splitting, leads to a z-polarization component for the transition in which MCD appears. The first ligand field transition in  $C_{2v}$  site symmetry ( $A_1 \rightarrow A_1$ ) is in fact predicted to be accessible in z-polarization, satisfying the requirement for a z-polarization component in MCD active transition originating in the  $M_S = 0$  sublevel. However, the presence of a z-polarization component by itself is not sufficient, since MCD intensity requires the presence of two nonvanishing components of the electric dipole transition moments in a transition. This was shown clearly by Gerstman and Brill,<sup>50</sup> through expansion of the expression for C-term MCD intensity in low symmetry:

$$\Delta\epsilon_{L-R} \propto g_x M_y M_z + g_y M_z M_x + g_z M_x M_y \quad (3)$$

This expression implies that C-term MCD intensity will vanish as orbital degeneracies are lifted unless some mechanism exists for mixing polarizations. Spin-orbit coupling among ligand field excited states leads to mixed polarization in transition to the coupled states and provides a mechanism for MCD intensity. Gerstman and Brill have also derived a sum rule<sup>50</sup> for the MCD intensity pattern over the excited-state spectra that applies for a set of states coupled through spin-orbit interactions but only weakly coupled to the ground state: The sum of MCD intensities over spin-orbit coupled excited states vanishes. Application of the sum rule to the opposite and nearly equal MCD intensity appearing in the first and third ligand field transitions for  $\text{Mn}^{3+}\text{SD}$  (to  $d_{x^2-y^2}$  and  $d_{xy}$ ) leads to the conclusion that spin-orbit coupling within this pair of excited states dominates in the mechanism for MCD intensity. These states are actually expected to have a relatively large spin-orbit interaction, and while the transition to  $d_{xy}$  is formally forbidden by an electric dipole mechanism for a simple  $d \rightarrow d$  excitation in  $C_{2v}$ , admixture of out-of-d-shell character or a descent in symmetry will introduce components of electric dipole intensity into this transition. Experimentally there is no question that there is an electric dipole contribution in the third ligand field transition, on the basis of its intensity in absorption. Spin-orbit mixing of  $d_{x^2-y^2}$  and  $d_{xy}$  excited states will result in mixed polarization in each, providing a mechanism for the appearance of the characteristic pattern of MCD intensity observed for native  $\text{MnSD}$ . This analysis supports a strong trigonal component to the  $\text{Mn}^{3+}$  site, consistent with the interpretation of the crystallographic data. One of the interesting features of the analysis is that it provides a connection between the ground-state properties (saturation behavior of MCD implying positive zero-field splitting) and the pattern of MCD intensity over the excited-state spectra, on the basis of the appearance of MCD in a ligand field transition for which z-polarization is predicted.

Additional structure is revealed in the absorption derivative spectra of the  $\text{Mn}^{3+}$  form of  $\text{MnSD}$  (Figure 2), although it is recognizable in other data as well. One prominent feature, the notch appearing near 525 nm in the absorption spectrum, is also evident in the MCD spectrum and most likely represents a ligand field independent spin-forbidden transition on the basis of its narrow line width in absorption and MCD and its low intensity. The coincidence of a series of sharp features in this region near 500 nm in absorption derivative spectra both native and liganded forms of  $\text{Mn}^{3+}\text{SD}$  supports this assignment to components of a ligand field independent  $d \rightarrow d$  transition multiplet. Such features derive from spin pairing in electronic excited states, resulting in a manifold of ligand field states not represented in the simple diagram in Figure 12. Weak spin-forbidden ligand field independent transitions are in fact predicted for the  $\text{Mn}^{3+}$  ion in the visible region, suggesting an assignment of these features to components of the  ${}^5\Gamma \rightarrow {}^3G$  or  ${}^3H$  free ion multiplets. Both of these multiplets give rise to ligand field independent components in ligand field energy diagrams appropriate for tetragonal symmetry.<sup>51</sup> These triplet ligand field excited states occurring at low energy in  $\text{Mn}^{3+}$  complexes are inaccessible from the quintet ground state because of spin selection rules. However, spin-orbit coupling with nearby quintet excited states relaxes this restriction, as discussed earlier, and provides a mechanism for optical absorption and MCD intensity for these formally forbidden transitions.

The interaction of the active site Mn with exogenous ligands is an important aspect of its coordination chemistry directly relating to its catalytic function. Our results on interactions of the  $\text{MnSD}$  active site with  $\text{F}^-$  and  $\text{N}_3^-$  appear to be the first characterization of these complexes. Ligand binding to the  $\text{Mn}^{3+}$  site in SD has dramatic consequences only hinted at in absorption and CD spectra. The decrease in absorption intensity and the shift of  $\lambda_{\text{max}}$  to higher energy are consistent with a geometric distortion of the site on ligand binding, but the similarity of absorption spectra for the native and ligand complexes indicates

(50) Gerstman, B. S.; Brill, A. S. *J. Chem. Phys.* 1985, 82, 1212-1230.

(51) König, E.; Kremer, S. *J. Phys. Chem.* 1974, 78, 56-59.

that this must occur without dramatic shifts in the energies of ligand field states, suggesting that a relatively minor reorganization of the site is involved. The close correspondence, apart from the difference in intensity, of CD spectra for the native enzyme and ligand complexes also requires that the ligation changes do not result in large changes in ligand field energies. In particular, there is no change in the energy of the red band in the anion complexes, indicating that the coordination number of the site is not increased on ligand binding. This is of interest in terms of a recent interpretation of the electron density map of crystalline FeSD *Pseudomonas ovalis* FeSD (structurally homologous to MnSD) from X-ray diffraction studies, leading to a prediction of an unoccupied coordination position in the native enzyme,<sup>52</sup> presumably the site of anion coordination in complexes. The Mn site in *Thermus thermophilus* MnSD appears to have a weakly bound water molecule associated with the corresponding trigonal apical coordination site, and the electron density map for crystals of the azide complex appears to reflect the presence of both water and anion coordination to the metal ion in ligand complexes.<sup>9,10</sup> The spectroscopic data on anion complexes reported here does not appear to be consistent with either four-coordinate Mn<sup>3+</sup> in the native enzyme or a change in coordination number on anion binding, even for the second step of F<sup>-</sup> titration. Apparently this second, weak F<sup>-</sup> interaction does not involve direct complexation with the metal ion and may relate to a second anion binding site that has been suggested by perchlorate inhibition kinetics studies<sup>53</sup> and in the F<sup>-</sup> titration of FeSD.<sup>27</sup> Hopefully the combination of complementary approaches provided by crystallographic and spectroscopic studies may provide a clearer picture of ligand interactions in the active site complexes.

Insights into the nature of the perturbation associated with anion binding to the active site metal ion in MnSD are emerging from analysis of the spectroscopic data on these complexes. The two lowest energy spin-allowed ligand field bands are virtually unchanged in energy between native and anion complexes. The transitions at higher energy are most perturbed, and the dominant change appears to be a shift of the third d → d transition to higher energy, consistent with a geometric distortion of the active site metal complex toward the square-pyramidal limit. The dramatic intensity changes in absorption and CD may also reflect a geometric distortion through ligand field effects but could also easily derive from a change in charge transfer mixing in the ligand field spectra resulting from the ligation change. However, the argument for a structural transition toward square-pyramidal geometry is strengthened by an analysis of the MCD data recorded for the anion complexes.

The MCD saturation magnetization data (Figures 7 and 8) for the anion complexes contains information on their electronic ground states. Spectra recorded at equal magnetic field increments rapidly become independent of magnetic field strength, reflecting magnetic field saturation of MCD magnetization at high field. This behavior is associated with large Zeeman splittings developing within the lowest sublevels of the ground state, implying a large *g* value. In addition, the relatively small degree of nesting observed for the saturation magnetization curves for these complexes is characteristic of MCD originating within a nearly degenerate non-Kramers doublet ground state, labeled as  $M_S = \pm 2$  in Figure 12. The large Zeeman splitting within this doublet ( $g_{\text{eff}} = 8$ ) leads to the strong magnetic field saturation effects. A non-Kramers doublet lying lowest in an  $S = 2$  ground state is associated with negative zero-field splitting of the spin sublevels ( $D < 0$  in eq 2), which arises in the limit of  $d_{x^2-y^2}$  orbital ground state in tetragonal axial symmetry (Figure 13). MCD spectroscopy thus provides evidence for a change in the orbital ground state from  $d_{z^2}$  to  $d_{x^2-y^2}$  on anion binding, which follows naturally from the correlation from trigonal to square limiting geometries on the  $C_{2v}$  distortion path (Figure 12). It is interesting to note that the absorption and CD data alone are not able to provide this level of insight into

the nature of ground- and excited-state wave functions that is available in the MCD experiment. The details of the ground-state splitting can be further probed by applying the analysis we previously developed for MCD intensity originating in a non-Kramers doublet ground state,<sup>54</sup> leading to estimates for  $\delta$  (the rhombic zero-field splitting within the doublet sublevels) and the parallel component of the Zeeman splitting. For the fluoride complex, we obtain estimates of the ground-state parameters  $\delta = 2.7 \text{ cm}^{-1}$  and  $g_{\parallel} = 7.3$ , and for the azide complex,  $\delta = 2.2 \text{ cm}^{-1}$  and  $g_{\parallel} = 7.3$ . In each case, the large doublet splitting and *g* value below 8 indicate a significant rhombic distortion of the site, which again reflects deviations from axial behavior. From the magnitude of rhombic splitting  $\delta$ , a minimum value of the axial zero-field splitting can be estimated for the anion complexes,  $|D| = 2\text{--}3 \text{ cm}^{-1}$ , which is in the same range defined for the native Mn<sup>3+</sup> form by earlier magnetic susceptibility studies.<sup>22</sup> For comparison, tetragonal Mn<sup>3+</sup> sites in rutile are also found<sup>55</sup> to have a <sup>5</sup>B ( $d_{x^2-y^2}$ ) orbital ground state and inverted zero-field splitting,  $D = -3.4 \text{ cm}^{-1}$ .

The pattern of MCD intensity in the excited-state spectra for both F<sup>-</sup> and N<sub>3</sub><sup>-</sup> complexes of MnSD associates the majority of the signal with a pair of bands of opposite sign but nearly equal magnitude. This type of pattern was also encountered in the spectrum of native Mn<sup>3+</sup>SD and interpreted in terms of spin-orbit coupling among excited states and giving rise to a Brill sum rule<sup>50</sup> behavior for MCD intensities. The spectra of the native and anion complexes are however clearly different. A different set of transitions develops MCD intensity in the anion complexes compared to the native enzyme. The majority of the intensity appears in the highest (third and fourth) spin-allowed ligand field transitions in the ligand complexes, in contrast to the native enzyme where the strongest MCD intensity appears in the first and third ligand field excitations. The characteristic pattern shown in Figures 7 and 8 (top) is called a pseudo-A-term and is associated with near degeneracy of a pair of orbital states within which spin-orbit coupling is active. Referring to the ligand field energy diagram (Figure 12), the presence of an orbitally degenerate excited state at highest energy with an unquenched component of orbital angular momentum ( $L_z' = 1$ ) is associated with the square-pyramidal limiting geometry. This provides a second line of evidence for a change in geometry of the Mn site in Mn<sup>3+</sup>SD from trigonal toward square pyramidal on coordination of exogenous anions complementing the ground-state data. The surprising observation that both F<sup>-</sup> and N<sub>3</sub><sup>-</sup> anions with very distinct ligand characteristics, form complexes with such remarkably similar spectroscopic characteristics suggests that the MnSD active site imposes these changes on the complexes and that anion coordination in some way triggers a local conformational change involving the metal complex with the consequences reflected in the spectra shown here. This rearrangement need not be severe: Even a minor structural change in bond angles and bond lengths in the complex could lead to a change in the axis of spatial quantization (Berry pseudorotation), leading to a change in symmetry of the empty valence orbital on Mn<sup>3+</sup>, which is the redox active orbital involved in the reactivity of the active site complex. A similar pseudorotation of principal axes in the active site metal complex has been proposed for Cu/Zn SD from single-crystal EPR experiments<sup>56</sup> and crystallographic studies<sup>57</sup> and appears to be an important feature of the coordination chemistry of this active site. While the significance of this for active site chemistry has yet to be clearly demonstrated or defined, the possibilities for a mechanistically important structural isomerism of the active site metal complex is clearly of interest, especially in view of studies emphasizing the geometric mobility often associated with five-coordination.<sup>58</sup>

(54) Whittaker, J. W.; Solomon, E. I. *J. Am. Chem. Soc.* **1988**, *110*, 5329–5339.

(55) Gerritsen, H. J.; Sabrisky, E. S. *Phys. Rev.* **1963**, *132*, 1507–1512.

(56) Lieberman, R. A.; Sands, R. H.; Fee, J. A. *J. Biol. Chem.* **1982**, *257*, 336–344.

(57) Tainer, J. A.; Getzoff, E. D.; Richardson, J. S.; Richardson, D. C. *Nature* **1983**, *306*, 284–287.

(52) Stoddard, B. L.; Howell, P. L.; Ringe, D.; Petsko, G. A. *Biochemistry* **1990**, *29*, 8885–8893.

(53) Bull, C.; Fee, J. A. *J. Am. Chem. Soc.* **1985**, *107*, 3295–3304.

An important calibration for the MCD spectra of a square-pyramidal complex is provided by the pentacoordinate  $\text{MnCl}_5^{2-}$  anion, as shown in Figure 9. Crystallographic analysis of the  $\text{MnCl}_5^{2-}$  complex<sup>59</sup> defines a nearly exact square-pyramidal arrangement of chloride ligands in the complex. Earlier spectroscopic assignments of the electronic transitions from detailed polarized single-crystal optical experiments have been reported,<sup>60</sup> identifying the 400-nm band as a degenerate ligand to metal charge transfer transition and the 550-nm band as arising from the  $d_{x^2-y^2} \rightarrow d_{xz,yz}$  ( $B_1 \rightarrow E$ ) ligand field transition, allowed in  $xy$ -polarization. The ligand field spectra occur at significantly lower energy in the pentachloride complex than in the protein, which probably reflects a weaker ligand field associated with the pentachloro ligation, but the MCD behavior is analogous, and a pseudo-A-term signal is observed. No MCD is detected in the lower energy transitions in this high-symmetry complex, where transitions to  $A_1$  and  $B_2$  ligand field excited states occur. The temperature dependence of MCD intensity reflects the  $S = 2$  paramagnetic ground state of this complex, and the magnetic field saturation behavior is consistent with a nearly degenerate non-Kramers doublet lowest in the ground state ( $D < 0$ ). Applying the slope-intercept method to the experimental saturation magnetization data to determine a ground-state Zeeman factor<sup>61</sup> yields an estimate of  $g_1 = 7.9$ , consistent with a nearly degenerate non-Kramers doublet lowest in the ground state, implying  $D < 0$ . Magnetic susceptibility studies on the  $\text{MnCl}_5^{2-}$  anion have been reported<sup>62</sup> consistent with this inverted zero-field splitting assignment we have made on the basis of MCD saturation magnetization data. The close analogy between MCD spectra and ground-state properties of  $\text{Mn}^{3+}$ SD anion complexes and the  $\text{MnCl}_5^{2-}$  model provide additional support for the fundamental features arising in the interpretation of the protein spectra and confirm the assignment of the pseudo-A-term MCD in the anion complexes of  $\text{Mn}^{3+}$ SD to transitions within a nearly square pyramidal complex.

The extreme trigonal-bipyramidal limiting geometry is expected to give rise to a distinct pattern of MCD intensity and saturation behavior, different from either of the two cases we have experimentally observed. The  $\Delta M_J = \pm 1$  selection rule for MCD transitions and the  $\Delta M_L = \pm 1$ ,  $\Delta M_S = \mp 1$  selection rule for spin-orbit mixing with the  $M_L = 0$  ( $z^2$ ) ground state ( $A_1$ ) suggests that the largest intensity would appear as an A-term-like MCD signal in transitions to the components of the  $M_L = \pm 1$  ( $xz, yz$ ) orbital doublet excited state ( $E'$ ), which lies at the highest energy for a trigonal-bipyramidal  $\text{Mn}^{3+}$  complex with weak axial interactions (Figure 12). This might superficially resemble the type of spectrum we observe for anion adducts of  $\text{Mn}^{3+}$ SD but would have very different saturation behavior reflecting the positive zero-field splitting in the  $^5A$  ground state, providing a clear distinction from the spectral properties associated with square-pyramidal  $\text{Mn}^{3+}$  with its  $^5B_1$  ground state.

In summary, the  $\text{Mn}^{3+}$  site in SD exhibits distinctive spectroscopic features in the native enzyme and in anion complexes that strongly suggest a distortion of the site occurs on anion binding. The spectroscopic evidence for retention of five-coordination in the azide complex in combination with the crystallographic evidence for retention of water in the active site on anion binding suggests that an associative displacement of water occurs in forming the anion complex. Restrictions on accessibility of the metal center to exogenous ligands imposed by the protein structure will control the geometric consequences of ligand binding and could account for the strong similarity in perturbations resulting from binding anions as dissimilar as azide and fluoride. A modulation of metal-water interactions has previously been proposed as an important aspect of the redox chemistry of  $\text{FeSD}$ ,<sup>53,63</sup> providing

a mechanism for coupling electron and proton transfer steps. Our results suggest that exogenous ligand interactions may also affect metal-water bonding. While it is conceptually useful to refer the enzyme complexes to the extremes of either trigonal or square axial symmetries defining the limits of the Berry coordinate, the  $\text{Mn}^{3+}$  site shows evidence of significant rhombic distortions in ground- and excited-state splittings, and the relatively minor changes in excited state energies associated with anion coordination imply that the metal complexes all lie in the middle range of the correlation in Figure 12, with excursions toward trigonal geometry in the native enzyme and toward square-pyramidal structure in the anion adducts. The resulting changes in the nature of the orbital ground state may be important for the redox chemistry of the active site. The  $d_{x^2-y^2}$  ground state defines the redox orbital in the anion complexes, which will be oriented according to the strongest or weakest ligand interactions. On the basis of the crystal structure for the  $\text{MnSD}$  active site, the  $z$  axis would be expected to lie along the Mn-carboxylate bond, leading to favorable orbital overlaps with the exogenous ligand (e.g., superoxide anion) and facilitating inner-sphere electron transfer.

**Manganous ( $\text{Mn}^{2+}$ ) Superoxide Dismutase.** The Mn in superoxide dismutase is redox active in its catalytic mechanism, in which both  $\text{Mn}^{3+}$  and  $\text{Mn}^{2+}$  oxidation states participate. On reduction of the  $\text{Mn}^{3+}$  site, the absorption features characteristic of the oxidized protein are lost and absorption spectroscopy is unable to provide information on the reduced metal center. Although there are cases where CD spectroscopy is effective in detecting extremely weak ligand field spectra in proteins inaccessible in absorption, we have been unsuccessful in detecting the ligand field spectra of the high-spin  $\text{Mn}^{2+}$  ( $3d^5$ ) ion in reduced  $\text{MnSD}$  even at 7.5 mM active sites. This is not entirely surprising since  $\text{Mn}^{2+}$  is expected to have extinction coefficients<sup>37</sup> on the order of  $10^2$ – $10^1 \text{ M}^{-1} \text{ cm}^{-1}$ , which severely limits detectability in both absorption and CD. In MCD spectroscopy, however, we have been able to detect extremely weak signals in the reduced protein samples that are characteristic of a high-spin  $d^5$  metal ion. Although weak, they are still stronger by more than 1 order of magnitude than spectra of free  $\text{Mn}^{2+}$  in glycerol solution, providing a spectroscopic control for signals arising from  $\text{Mn}^{2+}$  dissociated from the protein. This, in combination with other controls for the stability of the  $\text{Mn}^{2+}$ SD complexes, provides convincing evidence that the signals in fact derive from the reduced active site rather than free manganous ion in solution. The absence of Fe in the samples, the reducing conditions of sample preparation, and the distinctive spectrum of  $\text{Fe}^{3+}$ SD rule out a contaminating Fe species as the origin of these signals. The relatively high intensities of the MCD spectra are consistent with the low-symmetry environment expected for a protein complex, which would relax the parity selection rules for the formally  $d \rightarrow d$  transitions. The sharp transitions we can detect in the MCD spectrum are assignable as ligand field independent  $^6A \rightarrow ^4A, ^4E$  transitions that are relatively insensitive to environment.<sup>34–37</sup> More informative features that occur at lower energy in  $d^5$  complexes ( $^6A \rightarrow ^4T_1, ^4T_2$ ) will clearly require higher sensitivity measurements for detection.

EPR spectra for the  $\text{Mn}^{2+}$  active site complexes (Figure 11) exhibit a large number of resonances at X-band, characteristic of ground states with moderate zero-field splittings. This complicates the interpretation compared to cases defined by either large or small zero-field splitting. For the former case ( $D \gg h\nu$ ), the Zeeman interaction ( $g\beta H$ ) may be considered a perturbation on the zero-field splitting, and for a sextet ground state the spin Hamiltonian leads to three well-isolated Kramers doublets and an effective spin  $S' = 1/2$  within each doublet. In this case, only intradoublet transitions are observed over the normal magnetic field range of an EPR experiment. For small zero-field splitting ( $D \ll h\nu$ ), the Zeeman interaction dominates and spectra are centered on the free electron  $g$  value with splittings defined by  $D$ . On the other hand, for  $D \approx h\nu$ , the microwave energy approaches the doublet spacing and the spectra become complicated

(58) Muetterties, E. L. *Acc. Chem. Res.* **1971**, *3*, 266–273.

(59) Bernal, I.; Elliott, N.; Lalancette, R. *Chem. Commun.* **1971**, 803–804.

(60) Bellitto, C.; Tomlinson, A. A. G.; Furlani, C. *J. Chem. Soc. A* **1971**, 3267–3271.

(61) Thomson, A. J.; Johnson, M. K. *Biochem. J.* **1980**, *191*, 411–420.

(62) Witten, E. H.; Reiff, W. M. *Inorg. Chim.* **1980**, *41*, 227–228.

(63) Stallings, W. C.; Metzger, A. L.; Patridge, K. A.; Fee, J. A.; Ludwig, M. L. *Free Rad. Res. Coms.* **1990**.

by magnetic field induced mixing, interdoublet transitions, and level crossings as the field is swept, making the simulation of powder spectra difficult in this case.

The EPR spectra for Mn<sup>2+</sup>SD appear to reflect a zero-field splitting comparable to the microwave energy at X-band. Comparison of the experimental EPR turning points with published plots of resonance conditions for an  $S = 5/2$  spin system calculated by Dowsing and Gibson<sup>64</sup> or by Aasa<sup>65</sup> suggest  $D \approx 0.3 \text{ cm}^{-1}$  for native Mn<sup>2+</sup>SD with near axial symmetry. In the azide complex,  $D$  appears to be significantly reduced, leading to the appearance of low-field transitions extending to the zero-field limit. This is an indication that the zero-field splitting is only slightly smaller than the microwave energy for an inhomogeneous zero-field splitting distribution.  $D$  cannot be accurately determined in this case without a more extensive study and multifrequency EPR measurements, but the actual values of  $D$  are in any case of less interest than the observation that they are all unusually large compared to those of typical inorganic Mn<sup>2+</sup> complexes. Our analysis suggests that they are 1 order of magnitude larger than found for hexaaquamanganese(II) or other roughly octahedral six-coordinate complexes<sup>66</sup> but similar to values observed for distorted or lower coordination number complexes.<sup>67,68</sup> It is likely that the unusually large zero-field splittings derive from the strong axial perturbation (large orbital splittings) in Mn<sup>2+</sup>SD where the metal ion appears to remain five-coordinate.<sup>10</sup> As mentioned earlier, the sensitivity of our MCD experiments has not yet been sufficient to detect the splittings in the low-lying <sup>4</sup>T<sub>1</sub> and <sup>4</sup>T<sub>2</sub> excited states that contribute to the ground-state splitting in the d<sup>5</sup> ion.<sup>36</sup> The decrease in the magnitude of  $D$  on anion binding is consistent with a change in structure of the metal complex on coordination of exogenous ligands. The changes in the EPR spectra for the Mn<sup>2+</sup>SD in the presence of exogenous anions shows that EPR spectroscopy can provide a probe of ligand interactions in the reduced complex and demonstrates that the Mn<sup>2+</sup> site coordinates small molecules.

(64) Dowsing, R. D.; Gibson, J. F. *J. Chem. Phys.* **1969**, *50*, 294–303.

(65) Aasa, R. *J. Chem. Phys.* **1970**, *52*, 3919–3930.

(66) Kuska, H. A.; Rogers, M. T. In *Radical Ions*; Kaiser, E. T.; Kevan, L., Eds.; Interscience: New York, 1968; pp 650–661.

(67) de Bolster, M. W. G.; Nieuwenhuijse, B.; Reedijk, J. Z. *Naturforsch.* **1973**, *28b*, 104–106.

(68) Birdy, R. B.; Brun, G.; Goodgame, D. M. L.; Goodgame, M. J. *Chem. Soc., Dalton Trans.* **1979**, 149–151.

Manganese has a single stable isotope (<sup>55</sup>Mn, 100% natural abundance) having a nuclear spin  $I = 5/2$ . Electron–nuclear hyperfine interactions arising from interaction of the unpaired electronic spin with the nuclear spin  $I = 5/2$  of the Mn ion lead to fine structure splittings in EPR of Mn complexes, appearing as a  $2I + 1 = 6$ -fold multiplet pattern containing additional ground-state information. For Mn<sup>2+</sup> ions in solution, this results in the characteristic six-line EPR spectrum near the free electron  $g$  value, which appears as a minority species in our spectra. Hyperfine structure can also be partly resolved in some on the spectra reported here for Mn<sup>2+</sup>SD species. For the native enzyme, the feature near  $g = 5.8$  exhibits a 6-fold splitting with  $a_{\text{Mn}} = 86 \text{ G}$  ( $A_{\text{Mn}} = 80 \times 10^{-4} \text{ cm}^{-1}$ ), which is in the range observed for Mn<sup>2+</sup> in weakly covalent sites ( $A_{\text{Mn}} = (80\text{--}95) \times 10^{-4} \text{ cm}^{-1}$ ) in oxide lattices and carboxylate complexes.<sup>66</sup>

**Concluding Remarks.** On the basis of a combination of powerful spectroscopic approaches, we have clear evidence for anion interactions with both oxidized and reduced active site metal centers in MnSD, a contrast with FeSD where MCD was unable to detect anion perturbations in the reduced form.<sup>54</sup> The coordination chemistry reflected in these perturbations is of particular interest in terms of the catalytic properties of the active site toward superoxide dismutation and inner- versus outer-sphere redox reactivity of the metal center. A complete description of the changes in the Mn site on forming anion complexes is still lacking, but what emerges from these spectroscopic studies is a picture of an active site metal complex undergoing electronic structural perturbation on binding exogenous ligands. This perturbation appears to be associated with a change in geometry that is particularly clearly reflected in the crossover from a  $d_{z^2}$  to a  $d_{x^2-y^2}$  ground state defined by the MCD experiments on the Mn<sup>3+</sup> protein. The role this plays in the catalytic mechanism of MnSD remains to be explored, but there are clearly possibilities for modulating metal–ligand interactions in this type of conformationally mobile active site.

**Acknowledgment.** We express our appreciation to Dr. Danièle Touati, Institut Jacques Monod, Université Paris VII, for generously providing the MnSD over-expressing strain of *E. coli* for these studies. This work was supported by NIH Grants GM42680 and RR04212 (to J.W.W.).

**Registry No.** MnSD, 9054-89-1; Mn, 7439-96-5; F<sup>-</sup>, 16984-48-8; N<sub>3</sub><sup>-</sup>, 14343-69-2.